# Noncovalent Interactions of $Ni^+$ with N-Donor Ligands (Pyridine, 4,4′-Dipyridyl, 2,2′-Dipyridyl, and 1,10-Phenanthroline): Collision-Induced Dissociation and Theoretical Studies†

**N. S. Rannulu and M. T. Rodgers***

*Department of Chemistry, Wayne State University, Detroit, Michigan 48202*

*Received: December 18, 2008; Revised Manuscript Received: February 27, 2009*

Kinetic-energy-dependent collision-induced dissociation (CID) of complexes of a variety of N-donor ligands (*N*-L) with $Ni^+$, $Ni^+(N\text{-L})_x$, is studied using guided ion beam tandem mass spectrometry. The N-donor ligands investigated include: pyridine, 4,4′-dipyridyl, 2,2′-dipyridyl, and 1,10-phenanthroline. For most of the $Ni^+(N\text{-L})_x$ complexes, CID results in endothermic loss of a single neutral *N*-L ligand as the primary dissociation pathway. Sequential dissociation of additional *N*-L ligands is observed at elevated energies for the pyridine and 4,4′-dipyridyl complexes containing more than one ligand. The cross-section thresholds for the primary dissociation pathways are interpreted to yield 0 and 298 K bond dissociation energies (BDEs) of the $Ni^+(N\text{-L})_x$ complexes after accounting for the effects of multiple ion−neutral collisions, the kinetic and internal energy distributions of the reactants, and their lifetimes for dissociation. Density functional theory calculations at the B3LYP/6-311+G(2d,2p)//B3LYP/6-31G* level are performed to obtain model structures, molecular parameters, and energetics for the neutral *N*-L ligands and the $Ni^+(N\text{-L})_x$ complexes. In general, theory is found to overestimate the strength of binding to the first *N*-L ligand, and underestimate the strength of binding to additional ligands. Trends in the sequential BDEs of the $Ni^+(N\text{-L})_x$ complexes are examined and compared to complexes of $Ni^+$, to several other ligands previously investigated. The trends in the sequential BDEs are primarily determined by the valence electronic configuration and the effects of sd-hybridization of $Ni^+$ but are also influenced by repulsive ligand−ligand interactions. Natural bond orbital analyses indicate that the binding in these complexes is primarily noncovalent.

## Introduction

Metal complexes of chelating ligands such as 2,2′-dipyridyl and 1,10-phenanthroline are of interest in metal coordination chemistry[1] and are among the most widely used chelating ligands in coordination chemistry in both the liquid and gas phases.[2] We have recently undertaken studies of the coordination behavior of late transition metal ions to these chelating ligands to examine how chelation interactions influence the geometry and strength of binding.[3] The coordination of $Ni^+$ to these chelating ligands, their building block, pyridine, and to 4,4′-dipyridyl, isostructural to 2,2′-dipyridyl, is reported here. In all cases, these ligands provide one or two $sp^2$-hybridized N atoms suitable for binding to a metal ion,[4] as shown in Figure 1. Also shown in the figure are the calculated and measured dipole moments and molecular polarizabilities of these ligands.[3,5−10] The metal ion complexes of these two chelating ligands have several features in common: both complexes are bidentate with $Ni^+$ bound to the two pyridyl N atoms. They differ slightly in their chelating abilities because of differences in the dipole moments, polarizabilities, $\pi$ acceptor abilities, and geometries of the free ligands. These chelating ligands show an increased preorganization and stronger binding energies as a result of the chelate effect compared to monodentate ligands.[11−14]

Metal complexes of these ligands have been investigated in the context of numerous biological applications,[15−18] environmental issues,[19,20] electrochemical applications,[21] and supramolecular chemistry.[22,23] Studies of the coordination chemistry of transition metal complexes with polypyridyl bridging ligands such as 4,4′-dipyridyl, 2,2′-dipyridyl, and 1,10-phenanthroline are also important because of their potential as building blocks for supramolecular assemblies directed by either metal coordination or other intermolecular electronic interactions.[24−26] 2,2′-Dipyridyl has been found to be quite useful for a variety of biological applications. Raphael et al. have synthesized peptide

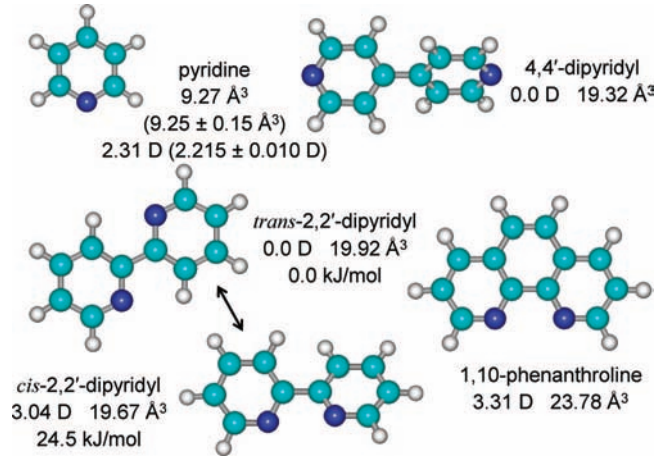


**Figure 1.** B3LYP/6-31G* optimized geometries of neutral pyridine, 4,4′-dipyridyl, 2,2′-dipyridyl, and 1,10-phenanthroline. Theoretical dipole moments and polarizabilities are taken from ref 3; experimental values are shown in parentheses and taken from refs 5−10. Relative energies of the cis- and trans-conformers of 2,2′-dipyridyl computed at the B3LYP/6-311+G(2d,2p) level of theory are also shown.

† Part of the "George C. Schatz Festschrift".

* Corresponding author. E-mail: mrodgers@chem.wayne.edu. Phone: 313-577-2431.

10.1021/jp8112045 CCC: $40.75 
Published on Web 03/12/2009

nucleic acid oligomers containing up to three adjacent 2,2′-dipyridyl ligands and examined their interactions with $Ni^{2+}$. They found that $Ni^{2+}$ binds to the ligands and increases the stability of the 2,2′-dipyridyl-modified duplex compared to that of the metal-free duplex. Variable temperature UV spectroscopy showed that duplexes containing a terminal pair of 2,2′-dipyridyl ligands are more stable upon metal binding than their nonmodified counterparts. Although binding of nonmetal ions to duplexes that contain two adjacent 2,2′-dipyridyl pairs make the duplexes more stable, additional metal ions lower the stability of the duplex, with electrostatic repulsion being a likely important contributor to the destabilization.[27,28]

The ligands 2,2′-dipyridyl and 1,10-phenanthroline are also used as antitumor compounds because of their chelating abilities. It has been demonstrated that dipyridyl derivatives inhibit cell growth by targeting the ribonucleotide reductase enzyme.[29] This enzyme plays a central role in DNA biosynthesis, furnishing a continuous and balanced supply of the four deoxyribonucleoside triphosphatases.[30] 1,10-Phenanthroline is also used as an antitumor drug because of its propensity to form stable complexes with metal ions and the possibility of intercalation of the aromatic portion of these complexes into the double helix of DNA.[31] Neutral diamine ligands, such as 2,2′-dipyridyl and 1,10-phenanthroline, have also been used as auxiliary ligands in electrospray ionization mass spectrometry to promote the formation of stable gas phase complexes involving divalent metal ions binding to ligands with an acidic hydrogen atom by occupying two coordinate sites of the metal and preventing the formation of neutral complexes of the type $[M^{2+}(L-H^+)_2]^0$ that would not be detected.[32−38]

In the current study, we examine noncovalent interactions between $Ni^+$ and multiple ligands of pyridine ($x = 1-4$), 4,4′-dipyridyl ($x = 1-4$), 2,2′-dipyridyl ($x = 1-3$), and 1,10-phenanthroline ($x = 1-3$). Collision-induced dissociation (CID) of these complexes is studied using guided ion beam tandem mass spectrometry techniques. The kinetic energy dependent cross sections for the primary CID processes are analyzed using methods developed previously.[39] The analysis explicitly includes the effects of the internal and translational energy distributions of the reactants, multiple ion−neutral collisions, and the lifetimes for dissociation. We derive $(N\text{–L})_{x-1}Ni^+(N\text{–L})$ BDEs and compare these results to values obtained from density functional theory calculations performed here. Comparison of the binding interactions of the monodentate ligands (pyridine and 4,4′-dipyridyl) with the chelating ligands (2,2′-dipyridyl and 1,10-phenanthroline) is employed to gain a better understanding of the influence that the number and orientation of the donor atoms and the size and flexibility of the ligands have upon the binding interactions. Examination of the trends in the sequential BDEs of these $Ni^+(N\text{-L})_x$ complexes as well as other $Ni^+(L)_x$ complexes previously investigated provide a more detailed understanding of the binding in these systems. Finally, natural bond orbital (NBO) analyses are used to further elucidate the nature of the binding in these systems.

## Experimental Section

**Experimental Protocol.** The guided ion beam tandem mass spectrometer employed for the experiments performed here has been described in detail elsewhere.[40] The $Ni^+(N\text{-L})_x$ complexes are formed by condensation of $Ni^+$, generated via dc discharge using a nickel cathode, with one or more neutral *N*-L ligands in a flow tube ion source. Of the *N*-L ligands examined here, 4,4′-dipyridyl, 2,2′-dipyridyl, and 1,10-phenanthroline are solids and were introduced into the flow tube by heating in a thermal probe (∼50−100 °C), located midway along the flow tube. Pyridine is a liquid and was directly introduced into the flow tube through a variable leak valve. These complexes are collisionally stabilized and thermalized by $>10^5$ collisions with the He and Ar bath gases, such that the internal energies of the $Ni^+(N\text{-L})_x$ complexes emanating from the flow tube are believed to be well described by a Maxwell−Boltzmann distribution at room temperature. The ions are effusively sampled from the source, focused, accelerated, and focused into a magnetic sector momentum analyzer for reactant ion mass selection. The mass-selected ions are decelerated to a desired kinetic energy by an exponential retarder and injected into an octopole ion beam guide. The octopole ion beam guide acts as an efficient radial ion trap such that loss of reactant and product ions as they drift through the octopole region is almost entirely eliminated.[41,42] The octopole passes through a static gas cell containing Xe at sufficiently low pressure (∼0.05−0.20 mTorr) that multiple ion−neutral collisions are improbable. Product and remaining reactant ions drift to the end of the octopole, are focused into a quadrupole mass filter for mass analysis, and are subsequently detected with a secondary electron scintillation (Daly)[43] detector using standard pulse counting techniques.

**Data Handling.** Ion intensities are converted to absolute cross sections using a Beer's law analysis as described previously.[44] Uncertainties in cross section magnitudes are estimated to be ±20% and are largely the result of uncertainties in the pressure measurement and length of the interaction region. Relative uncertainties are approximately ±5%.

Ion kinetic energies in the laboratory frame, $E_{Lab}$, are converted into energies in the center-of-mass frame, $E_{cm}$, using the formula $E_{cm} = E_{Lab}m/(m + M)$, where $M$ and $m$ are the masses of the ionic and neutral reactants, respectively. All energies reported below are in the center-of-mass frame unless otherwise noted. The absolute zero and distribution of the ion kinetic energies are determined using the octopole ion guide as a retarding potential analyzer as previously described.[44] The distribution of ion kinetic energies is nearly Gaussian with a fwhm in the range 0.3−0.4 eV (Lab) for these experiments. The absolute uncertainty in the energy scale is ±0.05 eV.

Because multiple ion−neutral collisions can influence the shape of CID cross sections and the threshold regions are most sensitive to these effects, each CID cross section was measured twice at three nominal Xe pressures (0.05, 0.10, and 0.20 mTorr). Data free from pressure effects are obtained by extrapolating to zero pressure of the Xe reactant, as described previously.[45] Thus, cross sections subjected to thermochemical analysis are the result of single bimolecular encounters.

**Theoretical Calculations.** Density functional theory calculations using the Gaussian03 suite of programs[46] were performed to obtain model structures, vibrational frequencies, rotational constants, and energetics for the $Ni^+(N\text{-L})_x$ complexes. In earlier work, we examined the analogous $Cu^+(N\text{-L})_x$ systems.[3] Therefore, results for the neutral ligands were taken from that work. Although experiments were only performed for the mono- and bis-complexes of 2,2′-dipyridyl and 1,10-phenanthroline, calculations were also performed for the tris-complexes to these ligands. Transition states for the interconversion of the cis- and trans-conformers of the $Ni^+$(2,2′-dipyridyl) complex were also calculated. Geometry optimizations and frequency analyses of the optimized structures were performed at the B3LYP/6-31G* level.[47,48] When used to model the data or to calculate thermal energy corrections, the B3LYP/6-31G* vibrational frequencies are prescaled by a factor of 0.9804.[49] The prescaled vibrational frequencies thus obtained for these systems are listed in the

Supporting Information in Table 1S, and Table 2S lists the rotational constants. Single point energy calculations were performed at the B3LYP/6-311+G(2d,2p) level using the B3LYP/6-31G* optimized geometries. Independent zero-point energy (ZPE) and basis set superposition error (BSSE) corrections are included in the calculated BDEs.[50,51]

NBO analyses of the $Ni^+$(pyridine), $Ni^+$(4,4′-dipyridyl), $Ni^+(pyridine)_2$, $Ni^+$(2,2′-dipyridyl), and $Ni^+$(1,10-phenanthroline) complexes were performed to gain insight into the nature of the binding in the $Ni^+(N\text{-L})_x$ complexes. The NBO program[52] in Gaussian03 performs the analysis of many-electron molecular wave functions in terms of localized electron pair "bonding" units, provides all possible interactions between filled Lewis-type electron-donor NBOs with unoccupied non-Lewis electron-acceptor NBOs, and estimates the stabilization energy associated with the electron donor−acceptor interactions, $E(2)$, using second order perturbation theory. The NBO analyses were performed at the B3LYP/6-311+G(2d,2p) level of theory using the B3LYP/6-31G* geometry optimized structures.

**Thermochemical Analysis.** The threshold regions of the CID cross sections are modeled using eq 1,

$$\sigma(E) = \sigma_0 \sum_i g_i(E + E_i - E_0)^n/E \qquad (1)$$

where $\sigma_0$ is an energy-independent scaling factor, $E$ is the relative kinetic energy of the reactants, $E_0$ is the threshold for reaction of the ground electronic and ro-vibrational state, and $n$ is an adjustable parameter that describes the efficiency of kinetic to internal energy transfer.[53] The summation is over the ro-vibrational states of the reactant ions, $i$, having energies, $E_i$, and populations, $g_i$, where $\Sigma g_i = 1$. We assume that the relative reactivity, as reflected by $\sigma_0$ and $n$, is the same for all ro-vibrational states.

The Beyer−Swinehart algorithm[54] is used to determine the density of ro-vibrational states, and the relative populations, $g_i$, are calculated for a Maxwell−Boltzmann distribution at 298 K, the internal temperature of the reactants. The vibrational frequencies are determined from electronic structure calculations as discussed in the Theoretical Calculations section. The average vibrational energy at 298 K of the neutral $N$-L ligands and $Ni^+(N\text{-L})_x$ complexes is given in the Supporting Information in Table 1S. We have increased and decreased the vibrational frequencies (prescaled by 0.9804) by 10% to encompass the range of averaging scaling factors needed to bring the calculated frequencies into agreement with experimentally determined frequencies.[55] The corresponding change in the average vibrational energy is used as an estimate for one standard deviation in the uncertainty in the vibrational energy (Table 1S, Supporting Information).

The dissociation of ions is expected to become slower as the size of the reactant ion and strength of the metal−ligand interaction increases. This leads to an increased probability that dissociation does not occur on the experimental time scale, $\sim 10^{-4}$ s for the experiments performed here. All CID processes faster than this are observed. However, as the lifetime of the energized molecule approaches this limit, the apparent CID threshold shifts to higher energies, a so-called *kinetic shift*. This kinetic shift is quantified and corrected for in our analysis by including statistical theories for unimolecular dissociation, specifically Rice−Ramsperger−Kassel−Marcus (RRKM) theory, into eq 1 as described in detail elsewhere.[39,56] This requires sets of ro-vibrational frequencies appropriate for the energized molecules and the transition states (TSs) leading to dissociation. We assume that the TSs are loose and product like because the interaction between $Ni^+$ and these $N$-L ligands is largely noncovalent. In this case, the molecular parameters of the TS used are those corresponding to the $Ni^+(N\text{-L})_{x-1}$ and $N$-L products, which are also provided in the Supporting Information in Tables 1S and 2S. The transitional frequencies, those that become translations and rotations of the completely dissociated products, are treated as rotors, a treatment that corresponds to the phase space limit (PSL) and is described in detail elsewhere.[39]

Equation 1 is convoluted with the kinetic energy distributions of the reactants, and a nonlinear least-squares analysis of the data is performed to give optimized values for the parameters $\sigma_0$, $E_0$, and $n$.[44] Uncertainties in the threshold values, $E_0$ and $E_0$(PSL), are determined from the range of threshold values for the zero-pressure-extrapolated data sets, variations associated with the vibrational frequencies (scaling as discussed above), and the uncertainty in the absolute energy scale, 0.05 eV (Lab). For analyses that include the RRKM lifetime analysis, the uncertainties in the reported $E_0$(PSL) values also include the effects of increasing and decreasing the time assumed available for dissociation ($\sim 10^{-4}$ s) by a factor of 2.

Equation 1 explicitly includes the internal energy of the reactant ion, $E_i$. All energy available is treated statistically because the ro-vibrational energy of the reactants is redistributed throughout the $Ni^+(N\text{-L})_x$ complex upon collision with the Xe atom. The threshold energies for dissociation reactions determined by analysis with eq 1 are equated to 0 K BDEs, which should be valid for the simple noncovalent bond cleavage reactions examined here.[57]

## Results

**Cross Sections for Collision-Induced Dissociation.** Experimental cross sections were obtained for the interaction of Xe with 12 $Ni^+(N\text{-L})_x$ complexes, where $N$-L = pyridine and 4,4′-dipyridyl and $x = 1-4$, and 2,2′-dipyridyl and 1,10-phenanthroline and $x = 1, 2$. Figure 2 shows representative data for the $Ni^+$(4,4′-dipyridyl)$_x$ and $Ni^+$(2,2′-dipyridyl)$_x$ complexes. Similar behavior is observed for $Ni^+(pyridine)_x$ and $Ni^+$(1,10-phenanthroline)$_x$ complexes; data for these systems are shown in the Supporting Information as Figure 1S.

**$Ni^+(pyridine)_x$ and $Ni^+$(4,4′-dipyridyl)$_x$.** The most favorable process for all of these monodentate complexes is the loss of a single intact $N$-L ligand in the CID reactions (2).

$$Ni^+(N\text{-L})_x + Xe \rightarrow Ni^+(N\text{-L})_{x-1} + N\text{-L} + Xe \qquad (2)$$

The cross section magnitudes increase, while the thresholds for reaction 2 decrease with increasing ligation, consistent with conventional ideas of ligation of gas phase ions;[58] i.e., stepwise sequential BDEs decrease because of increasing ligand−ligand repulsion and the decreasing effective positive charge retained by the metal ion. At elevated energies dissociation of additional $N$-L ligands is observed for the complexes containing more than one ligand. Ligand exchange to form $Ni^+Xe$ is observed only for the monoligated complexes, $Ni^+$(pyridine) and $Ni^+$(4,4′-dipyridyl).

**$Ni^+$(2,2′-dipyridyl)$_x$.** For the $Ni^+$(2,2′-dipyridyl) complex, in addition to simple CID to produce $Ni^+$ + 2,2′-dipyridyl (reaction 2), five activated dissociation pathways are observed and the total cross section exhibits two distinct features. The low-energy feature appears at an apparent threshold near 0.1 eV and arises from loss of neutral HCN to produce $Ni^+(C_9H_7N)$, reaction 3.

$$Ni^+(C_{10}H_8N_2) + Xe \rightarrow Ni^+(C_9H_7N) + HCN + Xe \quad (3)$$

Sequential dissociation of a second HCN molecule from the $Ni^+(C_9H_7N)$ product to produce $Ni^+(C_8H_6)$ is observed at an apparent threshold of 0.5 eV, reaction 4.

$$Ni^+(C_9H_7N) \rightarrow Ni^+(C_8H_6) + HCN \quad (4)$$

Three additional activated dissociation pathways leading to the elimination of neutral Ni(NCH) (or possibly Ni and HCN), $C_4H_2$, and $C_5H_5N$ from the reactant ion are also observed with apparent thresholds in the range 2.5−3.5 eV, reactions 5−7.

$$Ni^+(C_{10}H_8N_2) + Xe \rightarrow C_9H_7N^+ + Ni(NCH) + Xe \quad (5)$$

$$Ni^+(2,2'\text{-dipyridyl}) + Xe \rightarrow Ni^+(C_6H_6N_2) + C_4H_2 + Xe \quad (6)$$

$$Ni^+(2,2'\text{-dipyridyl}) + Xe \rightarrow Ni^+(C_5H_4N) + C_5H_4N + Xe \quad (7)$$

The simple CID pathway (reaction 2) exhibits the largest apparent threshold ~4 eV. The dual features in the cross section

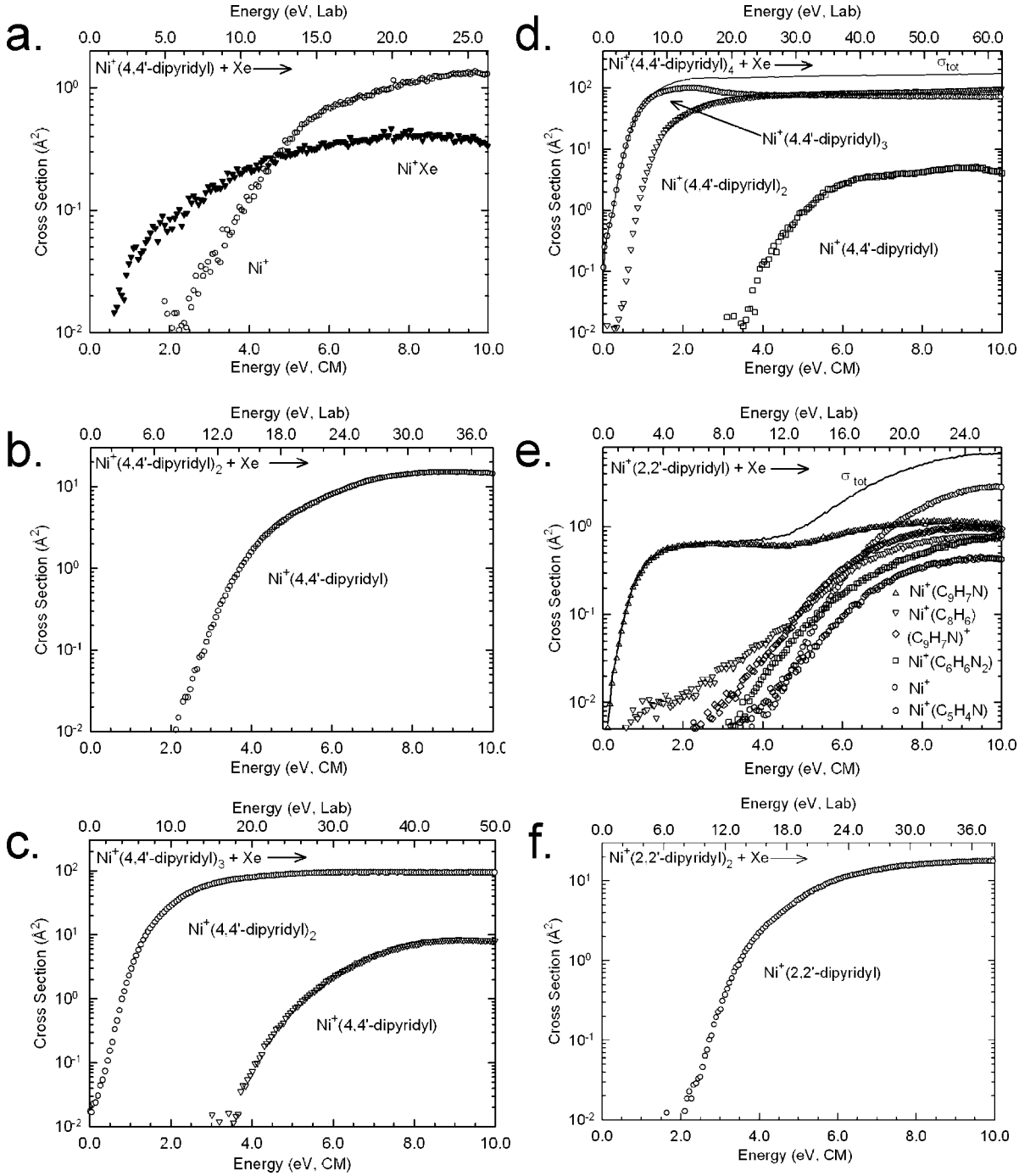


**Figure 2.** Cross sections for collision-induced dissociation of $Ni^+(4,4'\text{-dipyridyl})_x$ complexes, $x = 1-4$ parts a−d, and $Ni^+(2,2'\text{-dipyridyl})_x$ complexes, $x = 1$ and 2 parts e and f, respectively, with Xe as a function of kinetic energy in the center-of-mass frame (lower $x$-axis) and laboratory frame (upper $x$-axis). Data are shown for a Xe pressure of ~0.2 m Torr.

for reaction 3 and the total cross section and the complementarities of reactions 3 and 5 suggest that the reactant ion beam may be composed of more than one distinct structure, $Ni^+$(2,2′-dipyridyl), (HCN)$Ni^+(C_9H_7N)$, and/or $(HCN)_2Ni^+(C_8H_6)$. However, additional theoretical modeling would be needed to confirm this suggestion. Experimental attempts were made to investigate this possibility and eliminate the contaminant population but were unsuccessful.[59] Reaction 7 clearly corresponds to cleavage of the central C1−C1′ bond. The structures of the products of reaction 6 are not obvious, but it seems likely that the N2−C3 and C6−C1 bonds of one of the pyridyl rings are cleaved, two hydrogen atoms are transferred, and $C_4H_2$ departs as diacetylene.

In contrast to the complex behavior observed for the monocomplex, the CID of $Ni^+$(2,2′-dipyridyl)$_2$ is quite simple. Only simple CID (reaction 2) to produce $Ni^+$(2,2′-dipyridyl) is observed. Sequential dissociation to produce bare $Ni^+$ or the analogous activated dissociation pathways observed for the monocomplex are absent from the CID of the bis-complex over the range of collision energies examined. In particular, the absence of the activated dissociation pathway resulting in loss of HCN from $Ni^+$(2,2′-dipyridyl) in the CID of the bis-complex provides further support for the suggestion that more than one species is present in the reactant ion beam for the monocomplex. The lack of such a contaminant contributing to the reactant ion beam for the bis-complex, i.e., (HCN)$(C_9H_7N)Ni^+$(2,2′-dipyridyl) and/or $(HCN)_2(C_8H_6)Ni^+$(2,2′-dipyridyl) is likely the result of sd-hybridization effects that lead to very weak binding of the third and/or fourth ligand(s), HCN (see below). Consequently, this ion would not be expected to be formed with an appreciable population.

**$Ni^+$(1,10-phenanthroline)$_x$.** The CID behavior of the $Ni^+$(1,10-phenanthroline)$_x$ complexes is similar to that observed for the analogous $Ni^+$(2,2′-dipyridyl)$_x$ complexes. However, several of the activated dissociation pathways seen for $Ni^+$(2,2′-dipyridyl) are not observed in the CID of the $Ni^+$(1,10-phenanthroline) complex because of the very stable fused aromatic ring system. The total CID cross section for the $Ni^+$(1,10-phenanthroline) complex exhibits two distinct features. The low energy feature with an apparent threshold near 0 eV again arises from elimination of HCN from the reactant ion, reaction 8, in analogy to reaction 3 for the $Ni^+$(2,2′-dipyridyl) complex.

$$Ni^+(C_{12}H_8N_2) + Xe \rightarrow Ni^+(C_{11}H_7N) + HCN + Xe \quad (8)$$

Sequential dissociation of a second HCN molecule from the $Ni^+(C_{11}H_7N)$ product is observed at an apparent threshold of 0.5 eV, reaction 9, in analogy to reaction 4 for the $Ni^+$(2,2′-dipyridyl) complex.

$$Ni^+(C_{11}H_7N) \rightarrow Ni^+(C_{10}H_8) + HCN \quad (9)$$

Elimination of neutral Ni(NCH) is also observed with an apparent threshold of ∼2.0 eV, reaction 10, in analogy to reaction 5 for the $Ni^+$(2,2′-dipyridyl) complex.

$$Ni^+(C_{12}H_8N_2) + Xe \rightarrow (C_{11}H_7N)^+ + Ni(NCH) + Xe \quad (10)$$

The activated dissociation pathways analogous to reactions 6 and 7 are not observed as a result of the very stable fused aromatic ring system of 1,10-phenanthroline. The simple CID pathway (reaction 2) again exhibits the largest apparent threshold, ∼4.0 eV.

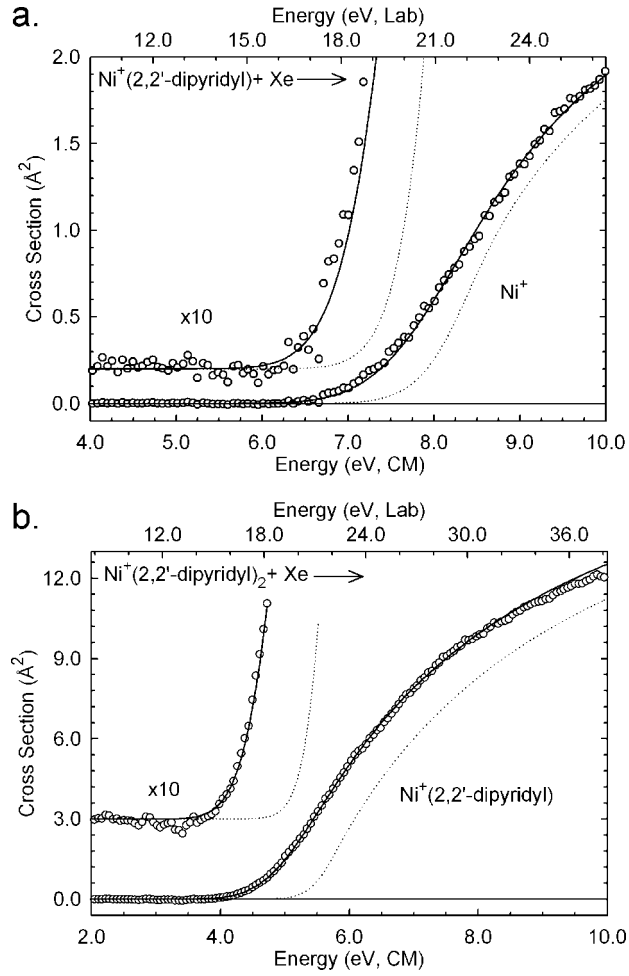


**Figure 3.** Zero-pressure-extrapolated cross sections for collision-induced dissociation of $Ni^+$(2,2′-dipyridyl)$_x$ complexes, $x = 1$ and 2 parts a and b, respectively, with Xe in the threshold region as a function of kinetic energy in the center-of-mass frame (lower $x$-axis) and laboratory frame (upper $x$-axis). Solid lines show the best fits to the data using eq 1 convoluted over the kinetic and internal energy distributions of the reactants. Dotted lines show the model cross sections in the absence of experimental kinetic energy broadening for reactants with an internal energy corresponding to 0 K.

Similar to that observed for the $Ni^+$(2,2′-dipyridyl) complex, CID of $Ni^+$(1,10-phenanthroline)$_2$ exhibits only simple CID (reaction 2) to produce $Ni^+$(1,10-phenanthroline) at an apparent threshold of ∼2.5 eV. The dual features in the cross section for reaction 8 and the total cross section for CID of $Ni^+$(1,10-phenanthroline), the complementarities of reactions 8 and 10, and the lack of the analogous activated dissociation pathways in the CID of the bis-complex again suggest that more than one species is present in the reactant ion beam for this system, i.e., $Ni^+$(1,10-phenanthroline), (HCN)$Ni^+(C_{11}H_7N)$ and/or $(HCN)_2Ni^+(C_{10}H_6)$.

**Threshold Analysis.** The threshold regions for reactions 2 in 12 $Ni^+(N\text{-L})_x$ complexes were analyzed using the model of eq 1. Good reproduction of the data is obtained over energy ranges exceeding 3.5 eV for all of the $Ni^+(N\text{-L})_x$ complexes. The zero-pressure-extrapolated CID cross sections and fits to the data using a loose PSL model for the interaction of $Ni^+$(2,2′-dipyridyl)$_x$, where $x = 1$ and 2, with Xe are shown in Figure 3. As can be seen in the figure, the cross sections for reaction 2, i.e., loss of the neutral $N$-L ligand, are accurately reproduced using a loose PSL TS model. Previous work has shown that this model provides the most accurate assessment of the kinetic

**TABLE 1: Fitting Parameters of Eq 1, Threshold Dissociation Energies at 0 K, and Entropies of Activation at 1000 K of $Ni^+(N\text{-}L)_x$ Complexes[a]**

| species | $\sigma_0$[b] | $n$[b] | $E_0$[c] (eV) | $E_0$ (PSL)[b] (eV) | kinetic shift (eV) | $\Delta S^\ddagger$ (PSL) (J $K^{-1}$ $mol^{-1}$) |
|---|---|---|---|---|---|---|
| $Ni^+$(pyridine) | 3.2 (0.6) | 1.3 (0.1) | 3.01 (0.06) | 2.70 (0.08) | 0.31 | 40.0 (2.0) |
| $Ni^+$(pyridine)$_2$ | 21.6 (0.7) | 1.4 (0.1) | 3.55 (0.05) | 2.59 (0.09) | 0.96 | 58.3 (4.4) |
| $Ni^+$(pyridine)$_3$ | 29.8 (1.4) | 1.2 (0.1) | 1.78 (0.03) | 1.47 (0.04) | 0.31 | 65.4 (4.5) |
| $Ni^+$(pyridine)$_4$ | 98.0 (1.3)[d] | 1.2 (0.1)[d] | 1.23 (0.1)[d] | 0.90 (0.02)[d] | 0.33[d] | 63.1 (4.6)[d] |
| $Ni^+$(4,4′-dipyridyl) | 1.6 (0.2) | 1.2 (0.1) | 4.27 (0.14) | 2.74 (0.11) | 1.53 | 36.8 (2.0) |
| $Ni^+$(4,4′-dipyridyl)$_2$ | 14.4 (2.8) | 1.5 (0.1) | 5.05 (0.12) | 2.53 (0.11) | 2.52 | 55.2 (4.4) |
| $Ni^+$(4,4′-dipyridyl)$_3$ | 68.9 (9.1) | 1.3 (0.1) | 2.52 (0.13) | 1.39 (0.06) | 1.13 | 62.0 (4.4) |
| $Ni^+$(4,4′-dipyridyl)$_4$ | 128.2 (22.6)[d] | 1.3 (0.1)[d] | 2.14 (0.04)[d] | 0.79 (0.03)[d] | 1.35[d] | 64.5 (4.5)[d] |
| $Ni^+$(2,2′-dipyridyl) | 11.4 (0.9) | 1.0 (0.1) | 6.55 (0.15) | 4.23 (0.14) | 2.32 | 51.8 (2.0) |
| $Ni^+$(2,2′-dipyridyl)$_2$ | 30.0 (1.9) | 1.1 (0.1) | 5.32 (0.09) | 2.81 (0.11) | 2.51 | 98.9 (4.4) |
| $Ni^+$(1,10-phenanthroline) | 1.2 (0.2) | 1.5 (0.1) | 7.45 (0.16) | 4.30 (0.12) | 3.15 | 59.8 (1.9) |
| $Ni^+$(1,10-phenanthroline)$_2$ | 42.1 (11.7) | 1.1 (0.3) | 5.90 (0.29) | 2.82 (0.12) | 3.08 | 95.4 (4.4) |

[a] Uncertainties are listed in parentheses. Average values obtained for fits to the primary product cross section except as noted. [b] Average values for loose PSL transition state. [c] No RRKM analysis. [d] Average values obtained for fits to the total cross section.

shifts for CID processes of electrostatically bound ion−molecule complexes.[58−61] The threshold analyses of the other $Ni^+(N\text{-}L)_x$ complexes are shown in the Supporting Information as Figure 2S.

For the $Ni^+(N\text{-}L)_x$ complexes where $x = 4$, sequential dissociation processes lead to a high energy fall off in the primary product cross section. Thus, the analyses must include the effects of subsequent ligand loss. This can be achieved by using a simple statistical model that conserves angular momentum, as described in detail previously.[62] This model depends on $E_D$, the energy at which the secondary dissociation channel begins, and $p$, a parameter similar to $n$ in eq 1. This extended model was employed for the analyses of the $Ni^+$(pyridine)$_4$ and $Ni^+$(4,4′-dipyridyl)$_4$ complexes. Although the high-energy model has proven to be extremely useful in describing such subsequent dissociations, lifetime effects have not been incorporated in the model. Because such effects could be appreciable in these rather large complexes, the reliability of analyses that include this simple high-energy model is unclear. Therefore, analyses of the total CID cross sections were performed for the $Ni^+$(pyridine)$_4$ and $Ni^+$(4,4′-dipyridyl)$_4$ complexes. These latter analyses are probably the most reliable. The fitting parameters obtained from fits to the total cross sections are similar to those obtained from fits to the primary product cross sections, and the $E_0$(PSL) thresholds differed by <0.01 eV. Thus, only results for the analyses of the total cross sections are provided in Table 1 and are shown in the Supporting Information as Figure 2S.

In the $Ni^+$(2,2′-dipyridyl) system, competition among reactions 2−7 and in the $Ni^+$(1,10-phenanthroline) system, reactions 2 and 8−10, might be expected to influence the threshold determination. In these cases, the threshold determination for reaction 2, without explicit consideration of this competition may only provide an upper limit to the $Ni^+$−2,2′-dipyridyl and $Ni^+$−1,10-phenanthroline BDEs. However, if the activated dissociation pathways arise from a contaminant as suggested above, these activated dissociation pathways should not interfere with the accurate determination of the threshold for reaction 2, and accurate BDEs can be extracted. Explicit modeling of the competition requires the knowledge of the TSs for reactions 3−7 and 8−10, which are likely to be tight TSs. Such computations were not pursued here and only independent analyses of the simple CID pathways (reactions 2) were performed.

**Kinetic Shifts.** Two threshold energies, $E_0$ and $E_0$(PSL), are listed in Table 1 for each $Ni^+(N\text{-}L)_x$ complex. $E_0$ represents the threshold obtained for analyses that do not include RRKM lifetime effects, and $E_0$(PSL) corresponds to the threshold obtained when the RRKM lifetime analysis is included. The difference in $E_0$ and $E_0$(PSL) provides a measure of the kinetic shift associated with the finite time scale of our measurements ($\sim 10^{-4}$ s). The total number of heavy atoms and thus the number of low-frequency vibrational modes increases as the size of the complex increases. Therefore, the density of states of the dissociating complexes increases with size. The density of states also increases with energy. Thus, the observed kinetic shifts should directly correlate with the size of the complex and the threshold energy. Because the BDEs fall off with increasing ligation, a simple trend in the kinetic shifts is not observed (Table 1). The kinetic shifts for the monodentate complexes, $Ni^+$(pyridine)$_x$ and $Ni^+$(4,4′-dipyridyl)$_x$, increase significantly from $x = 1$ to 2, fall precipitously from $x = 2$ to 3, and then increase slightly from $x = 3$ to 4. Thus, the kinetic shifts are the largest for the bis-complexes, larger than for the monocomplexes because they possess a larger number of modes, and larger than for the more highly ligated complexes because the binding in the bis-complexes is much stronger. The kinetic shifts for the $Ni^+$(4,4′-dipyridyl)$_x$ complexes are larger than for the corresponding $Ni^+$(pyridine)$_x$ complexes as a result of the larger size of the 4,4′-dipyridyl ligand. Because of the very strong binding interaction relative to the corresponding $Ni^+$(4,4′-dipyridyl) complex, the $Ni^+$(2,2′-dipyridyl) complex exhibits a much larger kinetic shift. The observed kinetic shift for the $Ni^+$(2,2′-dipyridyl)$_2$ complex is similar to that observed for the $Ni^+$(4,4′-dipyridyl)$_2$ complex as a result of the similar BDE and number of vibrational modes available to these two systems. Of the complexes examined here, the largest kinetic shifts are observed for $Ni^+$(1,10-phenanthroline)$_x$ systems, consistent with these complexes exhibiting the strongest binding interaction and the largest number of vibrations for $x = 1$ and 2, Table 1. The trends in the kinetic shifts for the $Ni^+$(2,2′-dipyridyl)$_x$ and $Ni^+$(1,10-phenanthroline)$_x$ complexes indicate that the much stronger binding in the monocomplexes slows the unimolecular dissociation by an amount similar to that resulting from the increased number of vibrational modes present in the bis-complexes.

**Entropies of Activation.** The entropy of activation, $\Delta S^\ddagger$, provides a measure of the looseness of the TS and is also a reflection of the complexity of the system. It is determined from the molecular parameters used to model the energized molecule and TS for dissociation but also depends upon the threshold energy. Listed in Table 1, the $\Delta S^\ddagger$(PSL) values at 1000 K vary between 37 and 99 J $K^{-1}$ $mol^{-1}$ for the $Ni^+(N\text{-}L)_x$ complexes examined here. The entropies increase with the size of the complex, i.e., as $x$ increases for a given $N$-L ligand, and for a fixed value of $x$ as the size of the $N$-L ligand increases. $\Delta S^\ddagger$ is

**TABLE 2: Bond Dissociation Energies of $Ni^+(N\text{-}L)_x$ Complexes at 0 K in kJ/mol**

| complex | experiment TCID[a] | theory $D_0$[b] | theory $D_{0,BSSE}$[c] |
|---|---|---|---|
| $Ni^+$(pyridine) | 260.5 (7.9) | 265.3 | 262.7 |
| | 254.8 (15.2)[d] | | |
| | 249.3 (15.7)[e] | | |
| $Ni^+(pyridine)_2$ | 250.6 (8.6) | 217.2 | 214.5 |
| $Ni^+(pyridine)_3$ | 141.8 (4.3) | 121.6 | 112.6 |
| $Ni^+(pyridine)_4$ | 86.7 (2.1) | 37.3 | 34.1 |
| $Ni^+$(4,4′-dipyridyl) | 264.2 (5.2) | 283.9 | 282.5 |
| $Ni^+(4,4'\text{-dipyridyl})_2$ | 244.3 (10.8) | 223.4 | 220.4 |
| $Ni^+(4,4'\text{-dipyridyl})_3$ | 134.7 (6.1) | 88.1 | 85.3 |
| $Ni^+(4,4'\text{-dipyridyl})_4$ | 76.4 (4.4) | 31.5 | 29.4 |
| $Ni^+$(2,2′-dipyridyl) | ≤407.9 (14.4)[f] | 421.2 | 418.3 |
| $Ni^+(2,2'\text{-dipyridyl})_2$ | 271.3 (10.8) | 225.1 | 220.4 |
| $Ni^+(2,2'\text{-dipyridyl})_3$ | | 17.3 | 13.1 |
| $Ni^+$(1,10-phenanthroline) | ≤414.7 (12.4)[f] | 453.7 | 449.3 |
| $Ni^+(1,10\text{-phenanthroline})_2$ | 272.1 (11.9) | 244.1 | 239.6 |
| $Ni^+(1,10\text{-phenanthroline})_3$ | | 47.5 | 43.4 |

[a] Present results, threshold collision-induced dissociation, except as noted. [b] Calculated at the B3LYP/6-311+G(2d,2p) level of theory using B3LYP/6-31G* optimized geometries. Including ZPE corrections with B3LYP/6-31G* frequencies scaled by 0.9804. [c] Also includes BSSE corrections. [d] Reference 62, TCID. [e] Reference 66, kinetic method adjusted to 0 K. [f] Upper limits to the experimental BDEs.

also larger for the chelating ligands than for the monodentate ligands as a result of the stronger and more geometrically constrained binding in the former complexes. These trends are expected on the basis of the complexity and the relative BDEs of these systems. The entropies of activation of these complexes also compare favorably to a wide variety of noncovalently bound complexes previously measured.[39,40,45,53,56,58−61,63−66,68−71]

**Theoretical Results.** Optimized geometries for the neutral *N*-L ligands and $Ni^+(N\text{-}L)_x$ complexes were calculated using Gaussian03[46] as described in the Theoretical Calculations section. BDEs calculated at the B3LYP/6-311+G(2d,2p)// B3LYP/6-31G* level of theory are listed in Table 2. ZPE and BSSE corrections are made for all complexes.

**Neutral *N*-L Ligands.** This work is a followup to an earlier study where we examined the analogous $Cu^+(N\text{-}L)_x$ systems.[3] As this work involves the same N-donor ligands, results for the neutral *N*-L ligands are taken from that work. Therefore, only a brief summary of the theoretical results for these neutral ligands is given here. The B3LYP/6-31G* optimized structures of the neutral *N*-L ligands along with their measured and calculated dipole moments and isotropic molecular polarizabilities are shown in Figure 1. The ground-state structures of pyridine, *trans*-2,2′-dipyridyl and 1,10-phenanthroline are planar, whereas the aromatic rings of 4,4′-dipyridyl and *cis*-2,2′-dipyridyl are twisted relative to each other. The dipole moment of pyridine is 2.215 ± 0.010 D (measured)[5] and 2.31 D (calculated).[3] 4,4′-Dipyridyl exhibits no net dipole moment because the local dipole moments cancel because of the symmetry of this ligand. Similarly, *trans*-2,2′-dipyridyl has no net dipole moment, but the local dipoles reinforce to produce a large dipole moment in the cis-conformer, 3.04 D. However, because the planes of the two rings are tilted by 35.1° with respect to one another, and it possesses a less extensive $\pi$ network, its dipole is smaller than that of 1,10-phenanthroline, which has the largest dipole moment among these ligands, 3.31 D.

Pyridine has the smallest polarizability among these ligands, 9.25 ± 15 Å$^3$ (measured)[6−10] and 9.27 Å$^3$ (calculated).[3] The polarizabilities of 4,4′-dipyridyl, *cis*-2,2′-dipyridyl, and *trans*-2,2′-dipyridyl are calculated to be 19.32, 19.67, and 19.92 Å$^3$, slightly more than twice as large as that of pyridine. The polarizability of 1,10-phenanthroline is the largest, 23.78 Å$^3$, in accord with it being the largest among these *N*-L ligands.[3]

**TABLE 3: Geometrical Parameters of the B3LYP/6-31G* Optimized Structures of the Neutral *N*-L Ligands and $Ni^+(N\text{-}L)_x$ Complexes[a]**

| species | bond length (Å) $Ni^+$−N | bond angle (deg) ∠NN$Ni^+$N | bond angle (deg) ∠XCCX[b] |
|---|---|---|---|
| $Ni^+$(pyridine) | 1.825 | | |
| $Ni^+(pyridine)_2$ | 1.846 (2) | 180.0 | |
| $Ni^+(pyridine)_3$ | 1.907 (2) | 103.1 (2) | |
| | 1.950 | 153.8 | |
| $Ni^+(pyridine)_4$ | 2.001 (2) | 98.2 (4) | |
| | 2.018 (2) | 135.5 (2) | |
| 4,4′-dipyridyl | | | 36.2 |
| $Ni^+$(4,4′-dipyridyl) | 1.823 | | 32.7 |
| $Ni^+(4,4'\text{-dipyridyl})_2$ | 1.862 (2) | 179.8 | 33.6 (2) |
| $Ni^+(4,4'\text{-dipyridyl})_3$ | 1.904 (2) | 103.1 (2) | 34.0 (3) |
| | 1.941 | 153.6 | |
| $Ni^+(4,4'\text{-dipyridyl})_4$ | 2.001 (4) | 98.1 (4) | 33.3 (2) |
| | | 135.7 (2) | 34.0 (2) |
| *trans*-2,2′-dipyridyl | | | 180.0 |
| *cis*-2,2′-dipyridyl | | | 35.1 |
| $Ni^+$(2,2′-dipyridyl) | 1.914 (2) | 92.4 | 24.3 |
| $Ni^+(2,2'\text{-dipyridyl})_2$ | 1.883 (4) | 85.0 (2) | 2.9 (2) |
| | | 109.6 | |
| | | 117.3 | |
| | | 133.5 (2) | |
| $Ni^+(2,2'\text{-dipyridyl})_3$ | 2.104 (6) | 78.3 (3) | 7.4 (2) |
| | | 89.4 (3) | 12.3 |
| | | 96.1 (6) | |
| | | 173.1 (3) | |
| 1,10-phenanthroline | | | 0.0 |
| $Ni^+$(1,10-phenanthroline) | 1.872 (2) | 92.5 | 0.0 |
| $Ni^+(1,10\text{-phenanthroline})_2$ | 1.976 (4) | 83.9 (2) | 0.8 |
| | | 105.0 (2) | |
| | | 147.8 (2) | |
| $Ni^+(1,10\text{-phenanthroline})_3$ | 2.107 (6) | 79.6 (3) | 2.2 (3) |
| | | 89.6 (3) | |
| | | 95.5 (6) | |
| | | 172.9 (3) | |

[a] Average values are given in cases where more than one bond distance or angle are similar, and degeneracies are given in parentheses. [b] Central ∠NCCN (2,2′-dipyridyl and 1,10-phenanthroline) or ∠CCCC (4,4′-dipyridyl) dihedral angle.

**$Ni^+(N\text{-}L)_x$ Complexes.** Optimized geometries for the $Ni^+(pyridine)_x$, $Ni^+(4,4'\text{-dipyridyl})_x$, $Ni^+(2,2'\text{-dipyridyl})_x$, and $Ni^+(1,10\text{-phenanthroline})_x$ complexes were computed at the B3LYP/6-31G* level of theory. Table 3 gives details of the final geometries for each of these species. The theoretical calculations find that in all of these complexes, $Ni^+$ prefers to bind to the lone pair(s) of electrons on the nitrogen atom(s) rather than the $\pi$ cloud of the aromatic ring(s). This preference for metal ion binding to the lone pair of electrons on the nitrogen atom(s) over binding to the $\pi$ cloud was previously observed for a wide variety of aromatic N-donor ligands.[3,60,63−66]

**$Ni^+(pyridine)_x$.** The ground-state structures of the $Ni^+(pyridine)_x$ complexes optimized at the B3LYP/6-31G* level of theory are shown in Figure 3S of the Supporting Information. In the $Ni^+$(pyridine) complex the $Ni^+$−N bond length is 1.825 Å. In the $Ni^+(pyridine)_2$ complex, the $Ni^+$−N bond lengths are slightly larger, 1.846 Å, primarily as a result of ligand−ligand repulsive interactions in the bis-complex. The ∠NN$Ni^+$N of the $Ni^+(pyridine)_2$ complex is 180° and the pyridine rings are oriented perpendicular to each other to minimize repulsive interactions between the pyridine ligands, and maximize stabilization gained via sd-hybridization of $Ni^+$, as discussed more fully below. The $Ni^+(pyridine)_3$ complex adopts a twisted

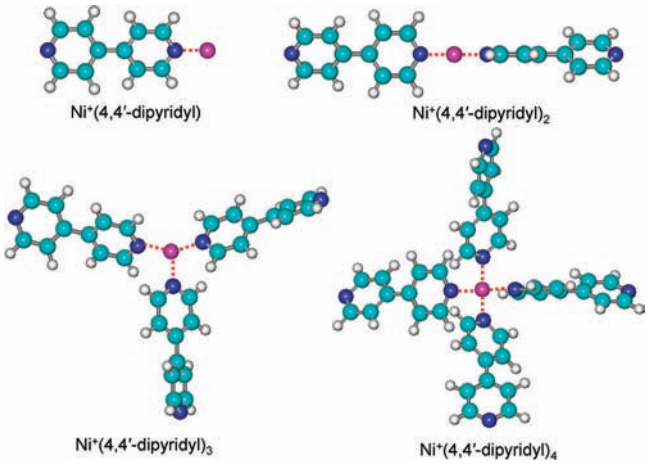


**Figure 4.** B3LYP/6-31G* optimized geometries of $Ni^+(4,4'\text{-dipyridyl})_x$ complexes, $x = 1-4$.

T-shaped propeller conformation, indicated by the ∠$NNi^+N$ bond angles, two of which are similar, ~103.1°, and the third is larger, ~153.8°. The T-shaped rather than equilateral triangle geometry arises from residual sd-hybridization of the orbitals on $Ni^+$. As a result, two of the $Ni^+-N$ bond lengths are equal, 1.907 Å and one is somewhat longer, 1.950 Å. The pyridine rings are twisted out of the plane of the N atoms by 43.8° to minimize ligand−ligand repulsive interactions. The $Ni^+(pyridine)_4$ complex is found to exhibit a distorted tetrahedral arrangement of the pyridine ligands around $Ni^+$ with two distinct $Ni^+-N$ bond lengths, 2.001 and 2.108 Å. However, the distorted tetrahedral geometry leads to different ∠$NNi^+N$ bond angles such that four similar, comparatively smaller bond angles (98.2°) and two larger bond angles (135.5°) are found. The distorted tetrahedral geometry again likely arises as a result of residual sd-hybridization of $Ni^+$. The pyridine rings are again twisted with respect to each other, by 30.8°, to minimize ligand−ligand repulsive interactions.

**$Ni^+(4,4'\text{-dipyridyl})_x$.** The B3LYP/6-31G* ground-state structures of the $Ni^+(4,4'\text{-dipyridyl})_x$ complexes are shown in Figure 4. The optimized geometries of the $Ni^+(4,4'\text{-dipyridyl})_x$ complexes are similar to those found for the $Ni^+(pyridine)_x$ complexes (compare Figures 4 and 3S, Supporting Information), as evidenced by comparable $Ni^+-N$ bond lengths and ∠$NNi^+N$ bond angles (Table 3). In neutral 4,4′-dipyridyl, the pyridyl moieties are twisted with respect to each other by 36.2° to minimize repulsion between the hydrogen atoms of the adjacent pyridyl rings. Upon binding to $Ni^+$, the dihedral angle between the two pyridyl moieties of the 4,4′-dipyridyl ligand reduces to 32.7° as a result of donation of electron density to $Ni^+$, thereby decreasing the electron density on the ligand and allowing a stronger binding interaction with the metal ion. The dihedral angle between the two pyridyl moieties of the 4,4′-dipyridyl ligands increases slightly but is not significantly altered by additional ligation (Table 3).

**$Ni^+(2,2'\text{-dipyridyl})_x$.** The B3LYP/6-31G* ground-state structures of the $Ni^+(2,2'\text{-dipyridyl})_x$ complexes are shown in Figure 5. In the ground-state conformation of neutral 2,2′-dipyridyl, the two pyridyl rings are coplanar and the two nitrogen atoms are located on opposite sides of the central C1−C1′ bond, i.e., the trans-conformer of 2,2′-dipyridyl shown in Figure 1. Complexation of 2,2′-dipyridyl to $Ni^+$ can occur directly to this conformation, but much stronger binding is achieved when the pyridyl rings rotate through the central C1−C1′ bond to orient both N atoms so that they may simultaneously interact with the $Ni^+$ ion. The rotation of the pyridyl rings results in a

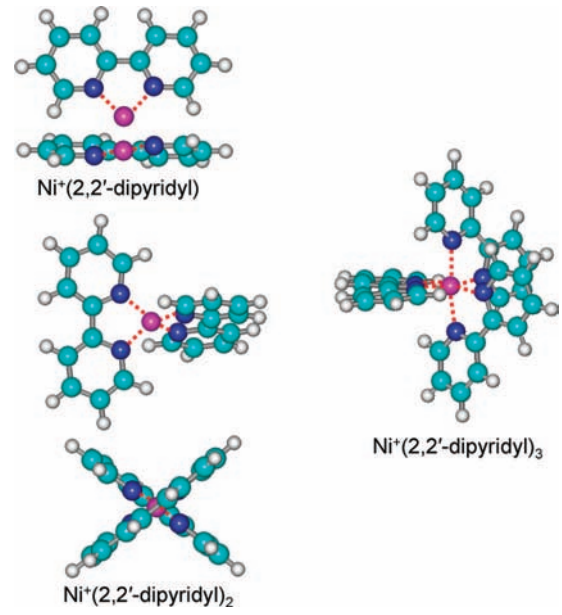


**Figure 5.** B3LYP/6-31G* optimized geometries of $Ni^+(2,2'\text{-dipyridyl})_x$ complexes, $x = 1-3$.

reduction of the ∠NCCN dihedral angle from 180° to 24.3°, somewhat smaller than the 35.1° dihedral angle in the cis-conformer of neutral 2,2′-dipyridyl. The ∠NCCN dihedral angle decreases further to 2.9° in the bis-complexes and increases to 7.4° for two of the ligands and 12.3° for the third in the tris-complex as a result of ligand−ligand repulsive interactions. The intramolecular ∠$NNi^+N$ bond angle in the monoligated complex is 92.4°, decreases to 85.0° in the bis-complex, and to 78.3° in the tris-complex. The $Ni^+-N$ bond lengths in $Ni^+(2,2'\text{-dipyridyl})$, 1.914 Å, are longer than that of $Ni^+(pyridine)_2$, 1.846 Å, and $Ni^+(4,4'\text{-dipyridyl})_2$, 1.862 Å. This is primarily a result of the steric restrictions in the former complex, and leads to the binding interaction in $Ni^+(2,2'\text{-dipyridyl})$ being weaker than the sum of the two binding interactions in the $Ni^+(pyridine)_2$ and $Ni^+(4,4'\text{-dipyridyl})_2$ complexes. The $Ni^+-N$ bond lengths decrease to 1.883 Å in $Ni^+(2,2'\text{-dipyridyl})_2$ and then increase to 2.104 Å in the $Ni^+(2,2'\text{-dipyridyl})_3$ complex. The $Ni^+(2,2'\text{-dipyridyl})_3$ complex exhibits a distorted octahedral structure with four N atoms nearly lying in a plane, whereas the other two N atoms lie above and below the plane.

**$Ni^+(1,10\text{-phenanthroline})_x$.** The B3LYP/6-31G* ground-state structures of the $Ni^+(1,10\text{-phenanthroline})_x$ complexes are shown in Figure 6. The binding geometry of the $Ni^+(1,10\text{-phenanthroline})$ complex is similar to that observed for $Ni^+(2,2'\text{-dipyridyl})$ except that the $Ni^+-N$ bonds lengths are slightly shorter, 1.872 Å versus 1.914 Å. The extended $\pi$ network of 1,10-phenanthroline remains planar when it interacts with $Ni^+$. However, the significant ligand−ligand repulsion results in distortion of the planar geometry of the 1,10-phenanthroline ligands in the bis- and tris-complexes such that the ∠NCCN dihedral angle increases to 0.8° and 2.2°, respectively. Similar to that observed for the $Ni^+(2,2'\text{-dipyridyl})_x$ complexes, the intramolecular ∠$NNi^+N$ angle decreases with increasing ligation, from 92.5° to 83.9° to 79.6° for the mono-, bis-, and tris-complexes as a result of the increasing $Ni^+-N$ bond distances. The $Ni^+-N$ bond distance of $Ni^+(1,10\text{-phenanthroline})_2$ is somewhat larger than that of the $Ni^+(2,2'\text{-dipyridyl})_2$ complex, and the $Ni^+-N$ bond distances are much closer in length in the tris-complexes. The $Ni^+(1,10\text{-phenanthroline})_3$ complex also exhibits a distorted octahedral structure similar to that of the $Ni^+(2,2'\text{-dipyridyl})_3$ complex.

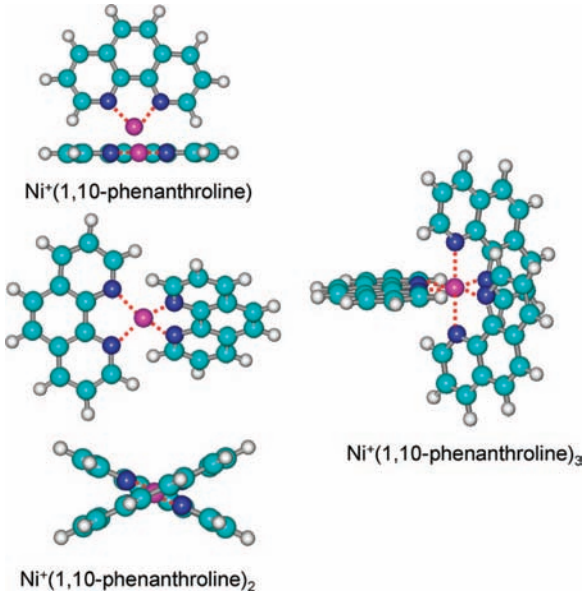


**Figure 6.** B3LYP/6-31G* optimized geometries of $Ni^+$(1,10-phenanthroline)$_x$ complexes, $x = 1-3$.

Trends in the $Ni^+-N$ bond lengths appear to be most closely linked to the flexibility of the ligand framework, rather than the relative bond strengths. The $Ni^+$(pyridine)$_x$ and $Ni^+$(4,4′-dipyridyl)$_x$ complexes exhibit comparable $Ni^+-N$ bond lengths that are shorter than those in the $Ni^+$(2,2′-dipyridyl)$_x$ and $Ni^+$(1,10-phenanthroline)$_x$ complexes. The more highly constrained geometry of the chelating ligands does not allow both N atoms to achieve optimal binding geometries with $Ni^+$ and results in slightly longer $Ni^+-N$ bond distances. The $Ni^+-N$ bond distance of $Ni^+$(1,10-phenanthroline) is slightly shorter than $Ni^+$(2,2′-dipyridyl), but still larger than the $Ni^+$(pyridine)$_x$ and $Ni^+$(4,4′-dipyridyl)$_x$ complexes. In $Ni^+$(1,10-phenanthroline)$_2$, the $Ni^+-N$ bond lengths are somewhat larger than in the corresponding $Ni^+$(2,2′-dipyridyl)$_2$ complex. The $Ni^+-N$ bond distances generally parallel the flexibility of these ligands, and therefore their ability to make structural changes to optimize the binding interactions. An exception to this behavior is observed for the $Ni^+$(2,2′-dipyridyl) and $Ni^+$(1,10-phenanthroline) complexes, which likely arises from the large dipole moment, polarizability, and $\pi$-acceptor abilities of 1,10-phenanthroline that allows the ligand to approach $Ni^+$ slightly more closely in spite of the constrained geometry of its planar $\pi$ network.

**NBO Analyses.** Natural bond orbital (NBO) analyses are employed to gain deeper insight into the nature of the binding interactions in the $Ni^+$(*N*-L)$_x$ complexes. NBO analyses were performed for the $Ni^+$(pyridine), $Ni^+$(4,4′-dipyridyl), $Ni^+$(pyridine)$_2$, $Ni^+$(2,2′-dipyridyl), and $Ni^+$(1,10-phenanthroline) complexes. The strength of the interaction of $Ni^+$ with these *N*-L ligands and the corresponding $E(2)$ stabilization energies were obtained between the electron donor and acceptor orbitals. Relevant orbital results are listed in Table 4. The most significant metal-to-ligand and ligand-to-metal donor−acceptor interactions of the $Ni^+$(pyridine)$_2$, $Ni^+$(2,2′-dipyridyl), and $Ni^+$(1,10-phenanthroline) complexes are shown in Figure 4S of the Supporting Information. The NBO analyses reveal that the dominant interactions arise from $\sigma$ donation of the lone pair of electrons of the pyridyl N atom, LP(N), to antibonding sd-hybridized orbitals on $Ni^+$, LP*(Ni). As can be seen in Figure 4S, these interactions look remarkably similar for these three complexes. The total $E(2)$ stabilization energies associated with the LP(N) → LP*(Ni) interactions are calculated to be 273.8, 275.6, 846.5, 425.8, and 483.2 kJ/mol for the $Ni^+$(pyridine), $Ni^+$(4,4′-dipyridyl), $Ni^+$(pyridine)$_2$, $Ni^+$(2,2′-dipyridyl), and $Ni^+$(1,10-phenanthroline) complexes, respectively. Given that the $E(2)$ stabilization energy for the $Ni^+$(pyridine)$_2$ complex is more than twice as large as that computed for the $Ni^+$(pyridine) complex suggests that the symmetry of this molecule may not be properly accounted for in the NBO analysis such that the $E(2)$ stabilization energies are overestimated by a factor of 2, or more appropriately ∼423.3 kJ/mol. This behavior may arise because the acceptor orbital on nickel is the same orbital for both ligands, and hence the factor of 2 may have been introduced by the degeneracy of the two ligands. Similar behavior was observed for the analogous $Cu^+$(pyridine)$_x$ complexes.[3] The stabilization energies for the complexes to the chelating ligands are significantly larger than for a single pyridine or 4,4′-dipyridyl ligand, but only slightly larger than for interaction of $Ni^+$ with two pyridine ligands, assuming that the factor of 2 correction is valid. Additional minor ligand-to-metal $\sigma$ donation interactions, BD(N−C) → LP*(Ni) and CR(N) → LP*(Ni), also contribute to the binding in these complexes. Metal-to-ligand $\pi$-back-donation also enhances the binding interactions between $Ni^+$ and these *N*-L ligands. The filled d orbitals of $Ni^+$ donate electron density to the antibonding orbitals of the pyridyl moieties, LP(Ni) → RY*(N) and LP(Ni) → BD*(N−C). These analyses indicate that 1,10-phenanthroline experiences stronger metal-to-ligand $\pi$-back-donation than 2,2′-dipyridyl or two pyridine ligands. The stabilization gained via $\pi$-back-donation from $Ni^+$ accounts for 7.1, 5.3, and 6.6% of the calculated stabilization for the $Ni^+$(pyridine), $Ni^+$(4,4′-dipyridyl), and $Ni^+$(pyridine)$_2$ complexes, respectively. In contrast, $\pi$-back-donation from $Ni^+$ accounts for 2.4 and 8.2% of the calculated stabilization for the $Ni^+$(2,2′-dipyridyl) and $Ni^+$(1,10-phenanthroline) complexes, respectively. The $\pi$-back-donation from $Ni^+$ to these *N*-L ligands is not as strong as that observed for the analogous $Cu^+$(*N*-L)$_x$ complexes,[3] which is likely the result of the longer $M^+-N$ bond distances in the complexes to $Ni^+$ (where the $Ni^+-N$ bond distances vary between 1.823 and 1.846 Å vs the $Cu^+-N$ bond distances that vary between 1.780 and 1.835 Å) that do not allow as effective an overlap of the associated orbitals. The more favorable $\pi$-back-donation from $Ni^+$ to 1,10-phenanthroline, as compared to 2,2′-dipyridyl or two pyridine ligands, arises because the filled d orbitals of $Ni^+$ overlap better with the $\pi^*$ orbitals of the planar $\pi$ network of 1,10-phenanthroline. Evidence for this can be seen in Figure 4S. The $Ni^+$(1,10-phenanthroline) complex exhibits stronger $\pi$-back-donation because the orbitals involved lie in the same plane as the complex, whereas in the $Ni^+$(2,2′-dipyridyl) complex these orbitals are not as well aligned with those of the ligands as a result of the twist in the pyridyl rings. The smaller difference in the $\pi$-back-donation between $Ni^+$(pyridine)$_2$ and $Ni^+$(1,10-phenanthroline) likely arises because both are well aligned to accept the $\pi$ electron density, but 1,10-phenanthroline has a more extensive $\pi$ network that tends to further stabilize these orbitals such that they lie closer in energy to the occupied orbitals of $Ni^+$ resulting in more effective overlap.

The NBO analyses also provide valuable information about the hybridization in these complexes. For example, the ground-state electron configuration of isolated $Ni^+$ is $4s^0 3d^9$. The natural electron configurations of $Ni^+$ in the $Ni^+$(pyridine), $Ni^+$(4,4′-dipyridyl), $Ni^+$(pyridine)$_2$, $Ni^+$(2,2′-dipyridyl), and $Ni^+$(1,10-phenanthroline) complexes are $4s^{0.39}3d^{8.76}$, $4s^{0.29}3d^{8.66}4p^{0.01}$, $4s^{0.53}3d^{8.75}4p^{0.01}$, $4s^{0.24}3d^{8.94}4p^{0.01}4d^{0.01}$, and $4s^{0.38}3d^{8.83}4p^{0.01}$,

**TABLE 4: Second-Order Perturbation Energies $E(2)$ (in kJ/mol) of Donor → Acceptor Interactions between $Ni^+$ and *N*-L Ligand(s) in $Ni^+(N\text{-L})_x$, Complexes at the B3LYP/6-311+G(2d,2p) Level of Theory[a]**

| | donor → acceptor interaction | | | | | |
|---|---|---|---|---|---|---|
| | ligand-to-metal σ-donation | | | metal-to-ligand π-back-donation | | |
| donor orbital: acceptor orbital: | LP(N) LP*(Ni) | BD(N−C) LP*(Ni) | CR(N) LP*(Ni) | LP(Ni) RY*(N) | LP(Ni) BD*(N−C) | total $E(2)$ stabilization |
| $Ni^+$(pyridine) | 115.4 | 5.6 | | 6.0 (2) | | 273.8 |
| | 133.4 | | | 7.4 | | |
| $Ni^+$(4,4′-dipyridyl) | 99.6 | 5.6 (2) | | | 7.9 | 275.6 |
| | 149.9 | | | | 6.9 | |
| $Ni^+(pyridine)_2$ | 335.1 (2) | 8.8 (4) | 5.3 (2) | 7.6 (2) | 6.1 (2) | 846.5 |
| | | 9.2 (2) | 5.5 (2) | 5.1 (2) | 9.2 (2) | *(423.3)*[b] |
| | | 26.9 | | | | |
| | | 9.1 (2) | | | | |
| $Ni^+$(2,2′-dipyridyl) | 196.7 (2) | 5.4 (2) | | | 5.2 (2) | 425.8 |
| | | 5.6 (2) | | | | |
| $Ni^+$(1,10-phenanthroline) | 78.8 (2) | | | 7.4 (2) | 5.3 (2) | 483.2 |
| | 58.4 (2) | | | | 6.3 | |
| | 84.5 (2) | | | | 8.1 | |

[a] Only $E(2)$ energies above 5.0 kJ/mol are shown. Orbital designations are defined as BD ≡ 2-center bond, CR ≡ 1-center core pair, LP ≡ 1-center lone pair, BD* ≡ 2-center unoccupied orbital, LP* ≡ 1-center unoccupied orbital, and RY* ≡ 1-center Rydberg orbital. Degeneracies of the donor → acceptor interactions are given in parentheses. [b] Total $E2$ stabilization assuming that the value is overestimated by a factor of 2.

respectively. These results clearly show that the 4s and 3d orbitals are hybridized to help minimize Pauli repulsion between $Ni^+$ and the *N*-L ligand(s). The 3d occupation of $Ni^+$ in the chelating ligand complexes is greater than in the complexes to the monodentate ligands, and the 4s occupation is the lowest for the dipyridyl ligands.

**Conversion from 0 to 298 K.** To allow comparison to commonly used experimental conditions, the 0 K BDEs determined here (experimentally and theoretically) are converted to 298 K bond enthalpies and free energies. The enthalpy and entropy conversions are calculated using standard formulas (assuming harmonic oscillator and rigid rotor models) and the vibrational and rotational constants determined for the B3LYP/6-31G* optimized geometries. Table 3S (Supporting Information) lists 0 and 298 K enthalpy, free energy, and enthalpic and entropic corrections for all systems studied. Uncertainties in the enthalpic and entropic corrections are determined by 10% variation in the molecular constants. Because theory may not adequately describe the weak interactions in these systems, the listed uncertainties also include contributions from scaling all frequencies below 150 $cm^{-1}$ up and down by a factor of 2. The latter provides a conservative estimate of the computational errors in these low frequency modes and is the dominant source of the uncertainties listed.

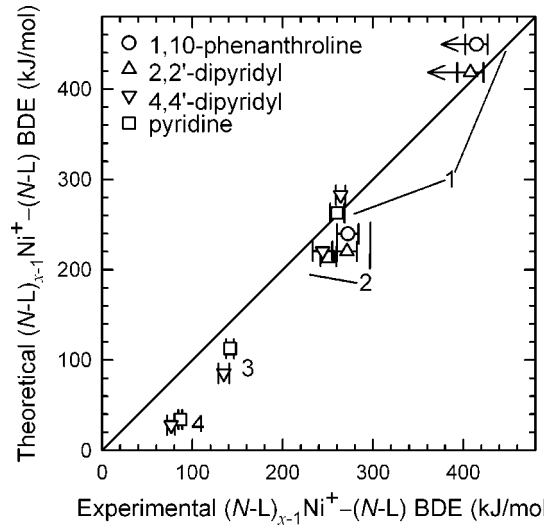


**Figure 7.** Theoretical versus experimental BDEs at 0 K (in kJ/mol) for $Ni^+(N\text{-L})_x$ complexes, where *N*-L include 1,10-phenanthroline (○), 2,2′-dipyridyl (△), 4,4′-dipyridyl (▽), and pyridine (□). The diagonal line indicates the values for which calculated and measured BDEs are equal.

## Discussion

**Comparison of Theory and Experiment.** The BDEs of the $Ni^+(N\text{-L})_x$ complexes, where *N*-L = pyridine and 4,4′-dipyridyl and $x = 1-4$, and 2,2′-dipyridyl and 1,10-phenanthroline and $x = 1$ and 2, were measured at 0 K by guided ion beam mass spectrometry. Table 2 lists the experimentally measured and theoretically calculated BDEs for all complexes. Figure 7 illustrates the agreement between the theoretically and experimentally determined BDEs for all of the $Ni^+(N\text{-L})_x$ complexes. As discussed in Threshold Analysis section, the BDEs determined for the $Ni^+$(2,2′-dipyridyl) and $Ni^+$(1,10-phenanthroline) may represent upper limits to the true BDEs as a result of the activated dissociation pathways observed that were not included in the threshold analyses. As can be seen in the figure, the agreement between theory and experiment is generally good. Theory slightly overestimates the strength of binding for all of the $Ni^+(N\text{-L})$ complexes except $Ni^+$(pyridine). In contrast, theory systematically underestimates the BDEs for all of the multiply ligated complexes, i.e., $Ni^+(N\text{-L})_x$, where $x > 1$.

**$Ni^+(pyridine)_x$.** The measured BDE of the $Ni^+$(pyridine) complex is in excellent agreement with the theoretical value. Table 2 also includes the experimental values for the $Ni^+$(pyridine) complex previously measured in our laboratory using the same threshold collision-induced dissociation (TCID) technique as employed here[63] and the value from the kinetic method work of Cooks et al.[67] The BDE for the $Ni^+$(pyridine) complex measured here is 5.7 kJ/mol larger than the value previously determined by TCID and in better agreement with theory but is still within experimental error of either measurement. In our earlier measurement, there was a low-energy feature we attributed to a small population of $Ni^+$(pyridine) present in an excited electronic state. We fit the data before and after subtracting out this low-energy feature and reported the threshold as the average threshold obtained from the two analyses. This

led to a threshold determination that was likely too low and less precise. Thus, the value measured here exhibits improved precision and should be more reliable. The BDE determined by the kinetic method is slightly lower than the TCID values but is also within experimental error of both measured values and the theoretical BDE. Thus, all three determinations of the $Ni^+$−pyridine BDE are clearly reliable. The calculated values for the $Ni^+(pyridine)_x$ complexes, where $x = 2-4$, are systematically lower than the experimentally determined values, by 36.1, 29.2, and 52.6 kJ/mol, respectively. A similar but slightly smaller discrepancy between the theoretical and experimental BDEs was also found for $Cu^+(N\text{-L})_x$ complexes where $x = 3$ and 4 to these ligands as well as to imidazole and acetone.[3−69] It is unclear why the agreement between theory and experiment is less satisfactory when the late transition metals, $Cu^+$ and $Ni^+$, bind to two or more ligands. A comparison of the experimental and theoretical BDEs determined at the B3LYP/6-311+G(2d,2p) level yields a mean absolute deviation (MAD) for the $Ni^+(pyridine)_x$ complexes of 30.0 ± 21.0 kJ/mol, significantly larger than the average experimental uncertainty (AEU) of 5.8 ± 2.6 kJ/mol for these complexes. The theoretical Gibbs free energy at 298 K for loss of pyridine from the $Ni^+(pyridine)_4$ complex is calculated to be negative, indicating a spontaneous process, which suggests that this complex is not bound at room temperature. This is clearly in direct conflict with our ability to observe $Ni^+(pyridine)_4$ and measure its CID behavior. This result suggests that the B3LYP/6-311+G(2d,2p) level of theory underestimates the strength of binding in the $Ni^+(pyridine)_4$ complex. Thus the disparity between the measured and calculated values and the observation of the $Ni^+(pyridine)_4$ complex, supports the suggestion that theory systematically underestimates the BDEs in the $Ni^+(pyridine)_x$ complexes, where $x \geq 2$.

**$Ni^+$(4,4′-dipyridyl)$_x$.** The BDEs of the $Ni^+(4,4'\text{-dipyridyl})_x$ complexes exhibit similar behavior to that observed for the $Ni^+(pyridine)_x$ complexes except that the experimental BDE of $Ni^+$(4,4′-dipyridyl) is lower than the theoretical BDE by 18.3 kJ/mol. As for the $Ni^+(pyridine)_x$ complexes, the theoretical BDEs of the $Ni^+(4,4'\text{-dipyridyl})_x$ complexes are consistently lower than the measured BDEs by 23.9, 49.4, and 47.0 kJ/mol for the $x = 2-4$ complexes, respectively. The MAD between the experimental and theoretical BDEs for the $Ni^+(4,4'\text{-dipyridyl})_x$ complexes is 34.6 ± 15.8 kJ/mol, significantly greater than the AEU in these BDEs, 6.7 ± 2.5 kJ/mol. As for the $Ni^+(pyridine)_4$ complex, theoretical calculations suggest that loss of neutral 4,4′-dipyridyl from the $Ni^+(4,4'\text{-dipyridyl})_4$ complex is a spontaneous reaction at 298 K. Clearly this is not the case, because again the experimental observation of this complex and its CID behavior suggest that this reaction is endoergic. Therefore, the less than satisfactory agreement between theory and experiment is again likely attributable to limitations in the level of theory used to describe these complexes.

**$Ni^+$(2,2′-dipyridyl)$_x$.** The BDE determined for the $Ni^+$(2,2′-dipyridyl) complex is 10.4 kJ/mol lower than the theoretical BDE. Although the value determined may represent an upper limit to the BDE, the fact that the measured value is lower than the computed value suggests that the activated dissociation pathways may indeed arise from a contaminant rather than from competitive dissociation of the $Ni^+$(2,2′-dipyridyl) complex, and thus the value measured here may represent an accurate measure of the $Ni^+$−2,2′-dipyridyl BDE. In contrast, the measured BDE for the $Ni^+(2,2'\text{-dipyridyl})_2$ complex exceeds the computed value by 51.3 kJ/mol. These results again suggest that the B3LYP/6-311+G(2d,2p) level of theory has difficulties accurately describing the binding in the multiply ligated complexes.

**$Ni^+$(1,10-phenanthroline)$_x$.** The BDE determined for the $Ni^+$(1,10-phenanthroline) complex is 34.6 kJ/mol lower than the theoretical value. Although the value measured may again represent an upper limit to the true BDE, it again seems likely that the activated dissociation pathways do indeed arise from a contaminant. Thus, the value determined likely represents an accurate measure of the $Ni^+$−1,10-phenanthroline BDE. In contrast, the measured BDE for the $Ni^+(1,10\text{-phenanthroline})_2$ complex is 32.5 higher than the theoretical value. These results again suggest that the B3LYP/6-311+G(2d,2p) level of theory is inadequate for accurately describing the binding in these complexes.

**Complexing Ability of the *N*-L Ligands.** Figure 1 shows the ground-state structures of the neutral *N*-L ligands along with their calculated and measured dipole moments and isotropic molecular polarizabilities. The ground-state structures of the $Ni^+(N\text{-L})_x$ complexes are shown in Figures 4−6 and Figure 3S (Supporting Information). In each of these complexes $Ni^+$ interacts with the lone pair(s) of electrons on the N atoms of the pyridyl rings rather than binding to the $\pi$ cloud of the aromatic rings. The strength and geometries of the binding in these $Ni^+(N\text{-L})_x$ complexes depend on the number of N-donor atoms, the $\pi$ acceptor ability, dipole moments, polarizabilities, and the flexibilities of these *N*-L ligands.

Both pyridine and 4,4′-dipyridyl are monodentate ligands and interact with $Ni^+$ via a single N atom of each ligand. Although 4,4′-dipyridyl possesses two donor centers, complexation occurs via a single N atom because the ligand is geometrically constrained such that only one N atom may bind to a given metal center. The chelating ligands, 2,2′-dipyridyl and 1,10-phenanthroline, have two donor centers that simultaneously interact with the metal ion and incorporate it into a ring, in both cases a relatively stable five-membered ring.

The ground-state conformation of 2,2′-dipyridyl is planar with the N atoms located on opposite sides of the central C−C bond, i.e., the trans-conformer. Rotation of the pyridyl rings through the central C−C bond such that both N atoms simultaneously interact with $Ni^+$ leads to a much stronger binding interaction. The potential energy landscape for the conversion of *trans*-2,2′-dipyridyl into *cis*-2,2′-dipyridyl was computed in our previous study of the analogous $Cu^+(N\text{-L})_x$ systems.[3] The energy barrier calculated for this conversion at 0 K is 28.9 kJ/mol relative to the ground-state trans-conformer. Figure 5S (Supporting Information) shows the potential energy landscape for this conversion in the presence of $Ni^+$. This conversion easily occurs because the internal energy of the initially formed $Ni^+$(*trans*-2,2′-dipyridyl) complex, 302.7 kJ/mol exceeds the barrier for interconversion of this species into the ground-state $Ni^+$(*cis*-2,2′-dipyridyl) complex, 147.0 kJ/mol relative to the $Ni^+$(*trans*-2,2′-dipyridyl) conformer. As can be seen in Figure 5, upon complexation of 2,2′-dipyridyl by $Ni^+$ the two pyridyl rings remain slightly twisted to minimize ligand−ligand repulsion, while retaining the maximum binding interaction between $Ni^+$ and the N-donor atoms. The three fused aromatic rings of 1,10-phenanthroline force this structure to be planar even after binding to $Ni^+$. However, ligand−ligand repulsion becomes significant enough to slightly distort the aromatic rings from planarity in the complexes involving more than one 1,10-phenanthroline ligand (Table 3).

These *N*-L ligands are strong $\sigma$ donors and weak $\pi$ acceptors. The lone pairs of electrons on the N atoms donate electron density into the sd-hybridized orbitals of $Ni^+$ (see discussion below), thus forming strong $\sigma$ bonds. Likewise, filled metal d orbitals donate electron density to the ligand $\pi^*$ orbitals and

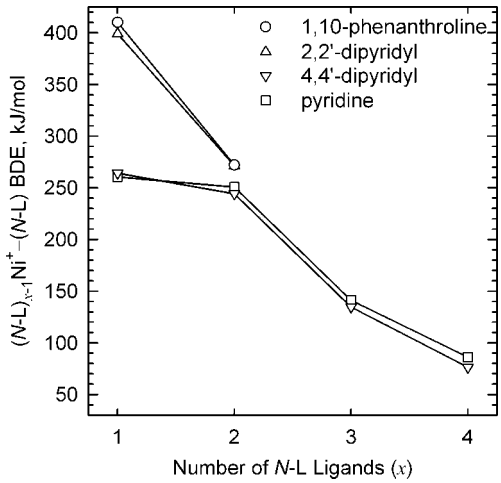


**Figure 8.** TCID measured $(N\text{-L})_{x-1}Ni^+(N\text{-L})$ BDEs at 0 K (in kJ/mol) as a function of the number of *N*-L ligands, *x*.

form d$\pi$-p$\pi$ backbonding. Both binding interactions act synergistically to produce very strong binding to $Ni^+$.

As a result of the similarity of these four ligands, the binding interaction of $Ni^+$ to these *N*-L ligands largely depends on the dipole moments and polarizabilities of the ligands. The dipole moment of pyridine is 2.31 D. The local dipole moments of each pyridyl ring of 4,4′-dipyridyl are expected to be very similar but cancel as a result of symmetry such that the net dipole moment of 4,4′-dipyridyl is 0.0 D. Thus, similar ion−dipole interactions are expected for the $Ni^+(pyridine)_x$ and $Ni^+(4,4'\text{-dipyridyl})_x$ complexes. The larger dipole moments of 2,2′-dipyridyl (3.04 D) and 1,10-phenanthroline (3.31 D) contribute to stronger binding interaction of these ligands to $Ni^+$ as compared to a single pyridine or 4,4′-dipyridyl ligand, but less than that expected for the binding of two monodentate ligands. The calculated molecular polarizabilities of pyridine, 4,4′-dipyridyl, *cis*-2,2′-dipyridyl, and 1,10-phenanthroline are 9.27, 19.32, 19.67, and 23.78 Å$^3$, respectively. Thus, the ion-induced dipole interactions are weakest for the $Ni^+(pyridine)_x$ complexes, almost twice as large for the $Ni^+(4,4'\text{-dipyridyl})_x$ and $Ni^+(2,2'\text{-dipyridyl})_x$ complexes, and nearly 2.5 times larger for the $Ni^+(1,10\text{-phenanthroline})_x$ complexes.

**Trends in the Sequential BDEs.** As can be seen in Figure 8, the bidentate ligands, 2,2′-dipyridyl and 1,10-phenanthroline, bind $Ni^+$ more strongly than the monodentate ligands, pyridine and 4,4′-dipyridyl. Similar behavior was observed in our previous study of the analogous $Cu^+(N\text{-L})_x$ complexes.[3] The second pyridine or 4,4′-dipyridyl ligand exhibits an unusually strong BDE as a result of sd-hybridization of $Ni^+$. Such sd-hybridization effectively removes electron density from the metal−ligand axis by placing the electron density in a hybridized orbital that is perpendicular to the bonding axis. This allows the ligand to approach $Ni^+$ with minimum repulsion energy. The BDE of the second ligand is nearly as strong as the first ligand, but slightly weaker. The weaker binding in the bis-complexes is likely the result of two effects, the decline in the effective positive charge retained by $Ni^+$ upon binding to the first ligand, and the repulsive interactions between the electron density of the first and second ligands.

The chelating ligands, 2,2′-dipyridyl and 1,10-phenanthroline, interact with $Ni^+$ via the lone pairs of electrons on both N atoms. Because these two N binding sites are constrained by the C−C backbone, they cannot optimally orient themselves around $Ni^+$, i.e., obtain a linear arrangement of the N−$Ni^+$−N atoms as found in the $Ni^+(pyridine)_2$ and $Ni^+(4,4'\text{-dipyridyl})_2$ complexes. To take full advantage of sd-hybridization of $Ni^+$, the ∠NN$i^+$N bond angle must be linear or close to 180°. The constrained ligand geometries of 2,2′-dipyridyl and 1,10-phenanthroline result in binding to $Ni^+$ with ∠NN$i^+$N bond angles of 92.4 and 92.5°, respectively. Therefore, less stabilization via sd-hybridization is achieved, resulting in less favorable binding than for two independent monodentate ligands.

The effects of sd-hybridization lead to much weaker binding of additional ligands beyond the first two for both pyridine and 4,4′-dipyridyl. A sharp decrease in the BDEs occurs for binding of the third ligand, whereas a fairly small decrease in the BDEs is observed from the third to the fourth ligand (Figure 8). Similar behavior has been observed for the binding of $Cu^+$ to these ligands[3] and of $Ni^+$ to several other ligands, e.g., $H_2O$,[45] $NH_3$,[70] CO, and $N_2$[71] (see discussion below).

The trends in the sequential BDEs of 2,2′-dipyridyl and 1,10-phenanthroline differ from that observed for the monodentate ligands, pyridine and 4,4′-dipyridyl. The BDEs for binding of the first ligand are very strong, and decrease sharply from the first to the second ligand, but are still quite strong. The more rapid decrease in the sequential BDEs for the complexes to 2,2′-dipyridyl and 1,10-phenanthroline arises because the electrostatic contributions to the binding decrease more rapidly upon sequential ligation because the chelating ligands provide two donor interactions such that the charge retained by $Ni^+$ decreases more rapidly than for the complexes to the monodentate ligands. The ligand−ligand repulsive interactions are also larger for these larger chelating ligands.

As can be seen in Figure 8, 4,4′-dipyridyl binds to $Ni^+$ slightly more strongly than pyridine as a result of the greater polarizability of the 4,4′-dipyridyl ligand. However, the sequential BDEs of 4,4′-dipyridyl decrease slightly more rapidly than those to pyridine because ligand−ligand repulsive interactions of the larger 4,4′-dipyridyl ligands overcome the effect of the enhanced binding arising from its larger polarizability.

1,10-Phenanthroline binds to $Ni^+$ slightly more strongly than 2,2′-dipyridyl. This suggests that the larger dipole moment, polarizability, and enhanced $\pi$-acceptor ability of 1,10-phenanthroline strengthen the binding interaction more than the flexibility of 2,2′-dipyridyl ligand. The sum of the binding energies for the first two pyridine and 4,4′-dipyridyl ligands to $Ni^+$ are essentially equal because the binding interactions are very similar and are dominated by sd-hybridization of $Ni^+$. The enhanced binding of the 4,4′-dipyridyl ligand arising from its larger polarizability is essentially canceled by the greater ligand−ligand repulsion of the 4,4′-dipyridyl ligands. The binding interaction of the first ligand of 2,2′-dipyridyl and 1,10-phenanthroline to $Ni^+$ is weaker than the sum of the first and second binding energies of the pyridine and 4,4′-dipyridyl by ∼25 and ∼24%, respectively. This larger difference results from reduced stabilization via sd-hybridization for the chelating ligands because of their constrained ligand geometries compared to two independent monodentate ligands. In contrast, $Ni^+$ binds the second 2,2′-dipyridyl and 1,10-phenanthroline ligand more strongly, by ∼16 and ∼23%, than the sum of the third and fourth BDEs to pyridine and 4,4′-dipyridyl. This suggests that these chelating ligands experience less ligand−ligand repulsion (two bidentate versus four monodentate ligands) as a result of their constrained ligand geometries. Furthermore, the third and fourth pyridine and 4,4′-dipyridyl ligands bind to $Ni^+$ less strongly because of the near complete loss of sd-hybridization.

The total energy required to completely dissociate the complexes to $Ni^+$ involving four $Ni^+$−N interactions into $Ni^+$ and neutral *N*-L ligands is fairly similar for all four *N*-L ligands,

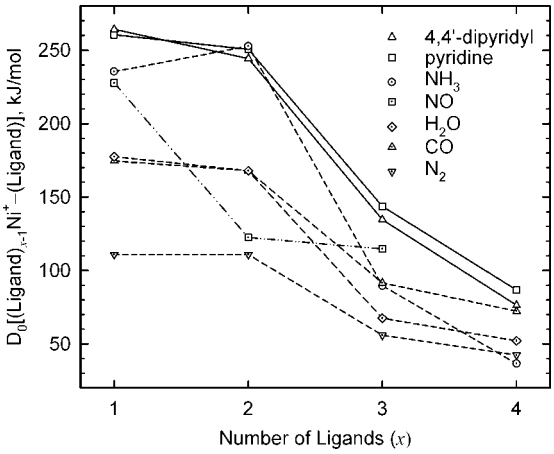


**Figure 9.** TCID measured $(Ligand)_{x-1}Ni^+(Ligand)$ BDEs at 0 K (in kJ/mol) as a function of the number of ligands, $x$. Values are taken from Table 2 for 4,4′-dipyridyl and pyridine and from ref 69 for $NH_3$, ref 45 for $H_2O$, and ref 70 for NO, CO, and $N_2$.

and follows the order $Ni^+(pyridine)_4 > Ni^+(4,4'\text{-dipyridyl})_4 > Ni^+(1,10\text{-phenanthroline})_2 \approx Ni^+(2,2'\text{-dipyridyl})_2$ complexes. This suggests that the constrained geometry of the chelating ligands weakens the binding more than it reduces ligand−ligand repulsive interactions.

**Comparison of $Ni^+$ and $Cu^+$ Binding Energies to N-Donor Ligands.** Besides $\sigma$ and $\pi$ charge transfer effects, sd-hybridization is found to be of critical importance in the interaction of these N-donor ligands to both $Ni^+$ and $Cu^+$. The trends in both the measured and calculated BDEs for these $Ni^+(N\text{-L})_x$ and $Cu^+(N\text{-L})_x$ complexes roughly parallel each other, but $Ni^+$ generally binds more strongly to these N-donor ligands than $Cu^+$. This likely arises because complete occupation of the d$\sigma$ orbital of $Cu^+$ ($d^{10}$) versus the half-filled d$\sigma$ orbital on $Ni^+$ ($d^9$) leads to less Pauli repulsion between the metal ion and ligand(s) for the $Ni^+(N\text{-L})_x$ complexes. Differences in the Pauli repulsion and the efficacy of sd-hybridization among these complexes also result in modest differences in their structures. In particular, the $Ni^+$−N bond distances are longer in the complexes involving one or two N-donor interactions than the corresponding $Cu^+$−N bond distances, suggesting that the sd-hybridization is more effective for the $Cu^+$ complexes than the $Ni^+$ complexes. In contrast, the $Ni^+$−N bond distances are shorter in the complexes involving three or four N-donor interactions than the corresponding $Cu^+$−N bond distances, suggesting that stabilization gained via sd-hybridization falls off more rapidly with ligation for the $Cu^+$ complexes than the $Ni^+$ complexes. This is also fairly evident in the monodentate complexes involving three or four N-donor ligands, where the $Ni^+$ systems exhibit geometries indicative of greater residual sd-hybridization of the orbitals on $Ni^+$ than the analogous $Cu^+$ systems. Indeed, population analyses indicate that the sd-hybridization is less complete for the $Ni^+(N\text{-L})$ complexes than for the corresponding $Cu^+(N\text{-L})$ complexes but diminishes less rapidly with increasing ligation.

**Comparison to Other Ligands.** As discussed above, the BDEs of $Ni^+(pyridine)_x$ and $Ni^+(4,4\text{-dipyridyl})_x$ complexes, where $x = 1, 2$, are quite strong and decrease somewhat from $x = 1$ to 2. A sharp decrease in the BDE is observed for $x = 3$, and then a fairly small decrease occurs for $x = 4$. Similar behavior has been observed in the sequential BDEs of several other ligands to $Ni^+$, i.e., $H_2O$,[45] $NH_3$,[70] CO, and $N_2$.[71] A comparison of the trends in the sequential BDEs of $Ni^+$ to these ligands is shown in Figure 9. As can be seen in the figure, the trends in the sequential BDEs for these $Ni^+(ligand)_x$ complexes are similar except that the relative binding strengths for the mono- and bis-complexes exhibit modest variation. The bis-ammonia complex binds more strongly, whereas the bis-dinitrogen complex binds equally, and the other bis-complexes bind somewhat less strongly than the corresponding monocomplexes. The reasons for these differences likely arise from differences in the ligand−ligand repulsion experienced in these systems as a result of differences in the $Ni^+$−ligand bond distances and the relative sizes of the ligands. The trends in the sequential BDEs of the $Ni^+(NO)_x$ complexes deviate significantly from the behavior seen for the other ligands. As can be seen in the figure, the binding of the second NO ligand is significantly weaker than the first. In the $Ni^+(NO)_2$ complex, the $Ni^+$−NO bond lengthens by 0.1 Å, resulting in a significant decrease in the strength of binding. In contrast, the bond lengths change by less than half as much for the other ligands upon going from the mono-complex to the corresponding bis-complex. In the interaction of $Ni^+(NO)$ with the second NO molecule, the N lone pair of the second NO ligand donates its electron density to the 4s orbital of $Ni^+$ and the $Ni^+$−N antibonding molecular orbital of $Ni^+(NO)$, which is responsible for the weakening of the second ligand.[72] In addition, $Ni^+(NO)$ is a singlet species such that the addition of the second NO ligand creates a radical, and hence the lower BDE is not surprisingly independent of the detailed molecular orbital interactions. Complexation of the third ligand of pyridine, 4,4′-dipyridyl, $NH_3$, CO, $H_2O$, and $N_2$ significantly decreases the BDEs as a result of the increased ligand−ligand repulsion and loss of stabilization arising from the sd-hybridization of $Ni^+$ as the third ligand interacts repulsively with the occupied sd-hybrid orbital. The behavior for the $Ni^+(NO)_3$ complex again differs with only a very small decrease in the BDE from the bis- to the tris-complex and is likely due to the fact that $Ni(NO_3)^+$ is an 18 electron species.[71]

The trends in the BDEs of these ligands are determined by the sum of the contributions arising from charge dipole, charge quadrupole, and charge-induced dipole interactions of these complexes. However, it is often the case that one of these terms is dominant. Therefore, it is useful to compare the trends in the BDEs to the dipole moments and polarizabilities of the ligands. The BDEs of $Ni^+$ to the first ligand follows the order 4,4′-dipyridyl > pyridine > $NH_3$ > NO > $H_2O$ > CO > $N_2$. NO is usually a three electron donor. In terms of the number of electrons donated by ligands, binding of NO to $Ni^+$ is expected to be stronger than $NH_3$, $H_2O$, CO, and $N_2$. However, as shown in Figure 9, binding of NO to $Ni^+$ is slightly weaker than to $NH_3$. The larger polarizability and dipole moment of $NH_3$ (4.48 Å$^3$, 3.92 D) enhances the binding interaction to $Ni^+$ as compared to NO (1.70 Å$^3$, 0.15 D). Even though pyridine (9.25 Å$^3$) and 4,4-dipyridyl (19.32 Å$^3$) are two electron donors, these ligands exhibit much stronger binding to $Ni^+$ as compared to $NH_3$ and NO due to the much larger polarizabilities of these two ligands. However, the dipole moments of pyridine (2.31 D) and 4,4-dipyridyl (0.0 D) are smaller than that of $NH_3$ (3.92 D), indicating that the ion-induced dipole interaction likely dominates the binding. The N-donor ligands bind more strongly to $Ni^+$ than O-donor ligands for both the mono- and bis-complexes. The binding of $H_2O$ to $Ni^+$ is slightly stronger than that of CO. The polarizability of CO is greater than that of $H_2O$ (1.95 Å$^3$ vs 1.45 Å$^3$), and therefore, the ion-induced dipole interaction is expected to be larger for CO than $H_2O$. Thus, the larger dipole moment of $H_2O$ as compared to CO (1.85 D vs 0.11 D) overcomes the polarizability differences and leads to stronger binding interactions.

## Conclusions

The kinetic energy dependences of the collision-induced dissociation of 12 $Ni^+(N\text{-}L)_x$ complexes, where *N*-L= pyridine and 4,4′-dipyridyl and $x = 1-4$, and 2,2′-dipyridyl and 1,10-phenanthroline and $x = 1$ and 2, with Xe are examined in a guided ion beam tandem mass spectrometer. The dominant dissociation process observed for all of the complexes is loss of a single neutral *N*-L ligand, assuming that the activated dissociation pathways observed for the $Ni^+$(2,2′-dipyridyl) and $Ni^+$(1,10-phenanthroline) complexes arise from contaminants. Thresholds at 0 K for these complexes are determined after consideration of the effects of the reactant internal energy, multiple collisions with Xe, and lifetime effects. Structures, theoretical estimates for the measured BDEs, and insight into the nature of the binding in the $Ni^+(N\text{-}L)_x$ complexes are provided by the density functional theory calculations. The B3LYP/6-311+G(2d,2p)//B3LYP/6-31G* theoretical BDEs of these $Ni^+(N\text{-}L)_x$ complexes exhibit similar trends but differ from the measured BDEs by more than the experimental uncertainty in these values for all complexes, except $Ni^+$(pyridine), where excellent agreement is found.

Our experimental results show that the chelating ligands, 2,2′-dipyridyl and 1,10-phenanthroline, exhibit very strong binding to $Ni^+$ as compared to a single monodentate ligand, pyridine or 4,4′-dipyridyl. The strong binding interaction of these chelating ligands primarily arises as a result of the bidentate interaction with the chelating ligands. However, the binding interaction of 2,2′-dipyridyl and 1,10-phenanthroline is weaker than the sum of two independent pyridine or 4,4′-dipyridyl ligands, a consequence of geometric restrictions that do not allow optimal orientation of the donor atoms around the $Ni^+$ ion. Therefore, these ligands cannot take full advantage of sd-hybridization. Binding of the second 2,2′-dipyridyl or 1,10-phenanthroline ligands is stronger than the sum of the third and fourth BDEs to pyridine because of the constrained ligand geometry of the chelating ligands leads to less ligand−ligand repulsion and sd-hybridization is still effective. The enthalpic contribution to the binding for all of the $Ni^+(N\text{-}L)_x$ complexes involving four N-donor interactions are nearly equal. Thus, the larger formation constants for the binding of metal−ligand complexes to the chelating ligands in solution[11−14] is almost entirely the result of entropic contributions to the binding.

NBO analyses performed for the $Ni^+$(pyridine), $Ni^+$(4,4′-dipyridyl), $Ni^+(pyridine)_2$, $Ni^+$(2,2′-dipyridyl), and $Ni^+$(1,10-phenanthroline) complexes reveal valuable information about the sd-hybridization and insight into the nature of the binding interactions in the $Ni^+(N\text{-}L)_x$ complexes. In all cases, the binding is dominated by $\sigma$ donation from the lone pairs on the N atoms and is thus primarily noncovalent. The binding is enhanced by $\pi$-back-donation from the *N*-L ligands to $Ni^+$, but its contribution to the binding is <10% in all cases.

**Acknowledgment.** This work is supported by the National Science Foundation, Grant CHE-0518262.

**Supporting Information Available:** Tables of vibrational frequencies, average vibrational energies at 298 K, rotational constants for the neutral *N*-L ligands and $Ni^+(N\text{-}L)_x$ complexes in their ground-state conformations, and enthalpies and free energies of binding of $Ni^+(N\text{-}L)_x$ complexes at 0 and 298 K. Figures showing cross sections for CID of $Ni^+(N\text{-}L)_x$ with Xe as well as empirical fits to the primary product channels for $x = 1-3$ and the total cross sections for $x = 4$ complexes, B3LYP/6-31G* optimized geometries of the $Ni^+(pyridine)_x$ complexes, the most significant donor → acceptor interaction of the $Ni^+$(pyridine), $Ni^+$(2,2′-dipyridyl) and $Ni^+$(1,10-phenanthroline) complexes, and the potential energy landscape for the association of $Ni^+$ with 2,2-dipyridyl and interconversion of the cis- and trans-conformers of $Ni^+$(2,2′-dipyridyl). This material is available free of charge via the Internet at http://pubs.acs.org.

## References and Notes

(1) Lehn, J. M. *Supramolecular Chemistry*, 1st ed.; Wiley VCH: Weinheim, 1995; p 295.
(2) Miller, K. S.; Chakraborty, T. A.; Sarkar, S.; Pradhan, B.; Sinha, B.; Kundu, R. K.; Ward, T.; Lahiri, M. D. *Dalton Trans.* **2003**, 2592–2596.
(3) Rannulu, N. S.; Rodgers, M. T. *J. Phys. Chem. A* **2007**, *111*, 3465–3479.
(4) Tsierkezos, N. G.; Diefenbach, M.; Roithova, J.; Schroeder, D.; Schwarz, H. *Inorg. Chem.* **2005**, *44*, 4469–4478.
(5) Nelson, R. D.; Lide, D. R.; Maryott, A. A. Selected Values of Electric Dipole Moments for Molecules in the Gas Phase. *Natl. Stand. Ref. Data. Ser.−Nat. Bur. Stnds.* **1967**, *10*, 49–104.
(6) *Landolt-Borstein, Atom und Molekularphysik*; Springer-Verlag: West Berlin, 1951; Vol. 1, Part 3, pp 511−513.
(7) LeFevre, C. G.; LeFevre, R. J. W.; Rao, B. P.; Smith, M. R. *J. Chem. Soc.* **1959**, 1188–1192.
(8) Sanyal, N. K.; Ahmad, P.; Dixit, L. *J. Phys. Chem.* **1973**, *77*, 2552–2556.
(9) Adams, S.; Nir, S.; Rein, R. *Int. J. Quantum Chem.* **1975**, *9*, 701–704.
(10) No, K. T.; Cho, K. H.; Jhon, M. S.; Scheraga, H. A. *J. Am. Chem. Soc.* **1993**, *115*, 2005–2014.
(11) Sammes, P. G. Yahioglu. G. *Chem. Soc. Rev.* **1994**, *23*, 327–334.
(12) Martell, A. E.; Hancock, R. D. *Metal Complexes in Aqueous Solution*, 1st ed.; Plenum Press: New York, 1996.
(13) Sigel, H., Sigel A., Ed. *Metal Ions in Biological Systems*; CRC Press, LLC Boca Raton, FL, 1988; Vol. 23, p 200.
(14) http://wwwchem.uwimona.edu.jm:1104/courses/chelate.html.
(15) Lehninger, A. L. *Biochemistry*, 3rd ed.; Worth Publishers: New York, 1996; p 438.
(16) Brody, F.; Ruby, P. R. In *Heterocyclic Compounds, Pyridine and Derivatives*; Klingsberg, E., Ed.; Interscience Publishers: New York, 1960; Part I, p 113.
(17) Veal, J. M.; Rill, R. L. *Biochem.* **1989**, *28*, 3243–3250.
(18) Sigman, D. S.; Bruice, T. W.; Mazumder, A.; Sutton, C. L. *Acc. Chem. Res.* **1993**, *26*, 98–108.
(19) Anipsitakis, G. P.; Dionysiou, D. D.; Malcolm, J.; Kestell, D. J. *Environmental* **2004**, *54*, 155–162.
(20) Tung, K.; Presley, B. *J. Anal. Chem.* **2002**, *74*, 4716–4724.
(21) Xu, G.; Dong, S. *Anal. Chem.* **2000**, *72*, 5308–5312.
(22) Saravanabharathi, D.; Samuelson, A. G. *Indian J. Chem.* **2003**, *42A*, 2300–2315.
(23) Vogtle, F. *Supramolecular Chemistry*, 2nd ed.; John Wiley & Sons: NewYork, 1991; p 172.
(24) Blake, A. J.; Champness, N. R.; Hubberstey, P.; Wan-Sheung, L.; Withersby, M. A.; Schröder, M. *Coord. Chem. Rev.* **1999**, *183*, 117–138.
(25) Leininger, S.; Olenyuk, B.; Stang, P. J. *Chem. Rev.* **2000**, *100*, 853–908.
(26) Kaes, C.; Katz, A.; Hosseni, M. W. *Chem. Rev.* **2000**, *100*, 3533–3590.
(27) Franzini, R. M.; Watson, R. M.; Patra, G. K.; Breece, R. M.; Tiernev, D. L.; Hendrich, K. P.; Anchim, C. *Inorg. Chem.* **2006**, *45*, 9798–9811.
(28) Wiederhott, K.; McLaughlin, L. *Nucleic Acids Res.* **1999**, *27*, 2487–2493.
(29) Nocentini, G.; Barzi, A. *Gen. Pharmac.* **1997**, *29*, 701–706.
(30) Reichard, P. *Science* **1993**, *260*, 1773–1777.
(31) Collins, J. G.; Rixon, R. M.; Aldrich-Wright, J. R. *Inorg. Chem.* **2000**, *39*, 4377–4379.
(32) Alvarez, E. J.; Vartanian, V. H.; Brodbelt, J. S. *Anal. Chem.* **1997**, *69*, 1147–1155.
(33) Satterfield, M.; Brodbelt, J. S. *Anal. Chem.* **2000**, *72*, 5898–5907.
(34) Alvarez, E. J.; Brodbelt, J. S. *J. Am. Soc. Mass Spectrom.* **1998**, *9*, 463–472.
(35) Pikulski, M.; Wilson, J. J.; Anguilor, A.; Brodbelt, J. S. *Anal. Chem.* **2006**, *78*, 8512–8517.
(36) Gatlin, C. L.; Turecek, F.; Vaisar, T. *J. Mass Spectrom.* **1995**, *30*, 1617–1627.
(37) Gatlin, C. L.; Rao, R. D.; Turecek, F.; Vaisar, T. *Anal. Chem.* **1996**, *68*, 263–270.
(38) Gerber, S. A.; Scott, C. R.; Turecek, F.; Gelb, M. H. *J. Am. Chem. Soc.* **1999**, *121*, 1102–1103.

(39) Rodgers, M. T.; Ervin, K. M.; Armentrout, P. B. *J. Chem. Phys.* **1997**, *106*, 4499–4508.
(40) Rodgers, M. T. *J. Phys. Chem. A* **2001**, *105*, 2374–2383.
(41) Teloy, E.; Gerlich, D. *Chem. Phys.* **1974**, *4*, 417–427.
(42) Gerlich, D. *Adv. Chem. Phys.* **1992**, *82*, 2202–2208.
(43) Daly, N. R. *Rev. Sci. Instrum.* **1960**, *31*, 264–267.
(44) Ervin, K. M.; Armentrout, P. B. *J. Chem. Phys.* **1985**, *83*, 166–189.
(45) Dalleska, N. F.; Honma, K.; Sunderlin, L. S.; Armentrout, P. B. *J. Am. Chem. Soc.* **1994**, *116*, 3519–3528.
(46) Frisch, M. J.; Trucks, G. W.; Schlegel, H. B.; Scuseria, G. E.; Robb, M. A.; Cheeseman, J. R.; Montgomery, J. A., Jr.; Vreven, T.; Kudin, K. N.; Burant, J. C.; Millam, J. M.; Iyengar, S. S.; Tomasi, J.; Barone, V.; Mennucci, B.; Cossi, M.; Scalmani, G.; Rega, N.; Petersson, G. A.; Nakatsuji, H.; Hada, M.; Ehara, M.; Toyota, K.; Fukuda, R.; Hasegawa, J.; Ishida, M.; Nakajima, T.; Honda, Y.; Kitao, O.; Nakai, H.; Klene, M.; Li, X.; Knox, J. E.; Hratchian, H. P.; Cross, J. B.; Adamo, C.; Jaramillo, J.; Gomperts, R.; Stratmann, R. E.; Yazyev, O.; Austin, A. J.; Cammi, R.; Pomelli, C.; Ochterski, J. W.; Ayala, P. Y.; Morokuma, K.; Voth, G. A.; Salvador, P.; Dannenberg, J. J.; Zakrzewski, V. G.; Dapprich, S.; Daniels, A. D.; Strain, M. C.; Farkas, O.; Malick, D. K.; Rabuck, A. D.; Raghavachari, K.; Foresman, J. B.; Ortiz, J. V.; Cui, Q.; Baboul, A. G.; Clifford, S.; Cioslowski, J.; Stefanov, B. B.; Liu, G.; Liashenko, A.; Piskorz, P.; Komaromi, I.; Martin, R. L.; Fox, D. J.; Keith, T.; Al-Laham, M. A.; Peng, C. Y.; Nanayakkara, A.; Challacombe, M.; Gill, P. M. W.; Johnson, B.; Chen, W.; Wong, M. W.; Gonzalez, C.; Pople, J. A. *Gaussian03*, revision D.01; Gaussian, Inc.: Pittsburgh, PA, 2003.
(47) Becke, A. D. *J. Chem. Phys.* **1993**, *98*, 5648–5652.
(48) Lee, C.; Yang, W.; Parr, R. G. *Phys. Rev. B* **1988**, *37*, 785–789.
(49) Foresman, J. B.; Frisch, A. E. *Exploring Chemistry with Electronic Structure Methods*, 2nd ed.; Gaussian: Pittsburgh, PA, 1996; p 64.
(50) Boys, S. F.; Bernardi, R. *Mol. Phys.* **1979**, *19*, 553–557.
(51) van Duijneveldt, F. B.; van Duijneveldt-van de Rijdt, J. G. C. M. *Chem. Rev.* **1994**, *94*, 1873–1885.
(52) Glendening, E. D.; Badenhoop, J. K.; Reed, A. E.; Carpenter, J. E.; Weinhold, F. *NBO Version 3.1*; Theoretical Chemistry Institute, University of Wisconsin: Madison, 1995.
(53) Muntean, F.; Armentrout, P. B. *J. Chem. Phys.* **2001**, *115*, 1213–1228.
(54) Beyer, T. S.; Swinehart, D. F. *Commn. ACM* **1973**, *58*, 2438–2445.
(55) Pople, J. A.; Schlegel, H. B.; Ragavachari, K.; DeFrees, K.; Binkley, D. J.; Frisch, J. F.; Whitesides, R. F.; Hout, R. F. H. *Int. J. Quant. Chem. Symp.* **1981**, *15*, 269–278.
(56) Khan, F. A.; Clemmer, D. E.; Armentrout, P. B. *J. Phys. Chem.* **1993**, *97*, 7978–7987.
(57) Armentrout, P. B.; Simons, J. *J. Am. Chem. Soc.* **1992**, *114*, 8627–8633.
(58) Rodgers, M. T.; Armentrout, P. B. *Mass Spectrom. Rev.* **2000**, *19*, 215–247.
(59) Variation of the temperature of the thermal probe did not alter the dissociation behavior and only served to decrease the reactant ion population. Unfortunately, we did not look for the formation of $Ni^+(C_9H_7N)$ and $Ni^+(C_{11}H_7N)$ in the flow tube ion source, whose formation would have lent further support for the presence of contaminants in the $Ni^+$(2,2′-dipyridyl) and $Ni^+$(1,10-phenanthroline) reactant ion beams.
(60) Amunugama, R.; Rodgers, M. T. *J. Phys. Chem. A* **2001**, *105*, 9883–9892.
(61) Rodgers, M. T.; Armentrout, P. B. *J. Phys. Chem. A* **1999**, *103*, 4955–4963.
(62) Weber, M. E.; Elkind, J. L.; Armentrout, P. B. *J. Chem. Phys.* **1986**, *84*, 1521–1529.
(63) Rodgers, M. T.; Stanley, J. R.; Amunugama, R. *J. Am. Chem. Soc.* **2000**, *122*, 10969–10978.
(64) Amunugama, R.; Rodgers, M. T. *Int. J. Mass. Spectrom.* **2000**, *195/196*, 439–457.
(65) Rodgers, M. T.; Armentrout, P. B. *Int. J. Mass. Spectrom.* **1999**, *185/186/187*, 359–380.
(66) Rannulu, N. S.; Amunugama, R.; Yang, Z.; Rodgers, M. T. *J. Phys. Chem. A* **2004**, *108*, 6385–6396.
(67) Wong, P. S. H.; Ma, S.; Wang, F.; Cooks, R. G. *J. Organomet. Chem.* **1997**, *539*, 131–139.
(68) Rannulu, N. S.; Rodgers, M. T. *Phys. Chem. Chem. Phys.* **2005**, *7*, 1014–1025.
(69) Chu, Y.; Yang, Z.; Rodgers, M. T. *J. Am. Soc. Mass Spectrom.* **2002**, *13*, 453–468.
(70) Walter, D.; Armentrout, P. B. *J. Am. Chem. Soc.* **1998**, *120*, 3176–3187.
(71) Khan, F. A.; Steele, D. L.; Armentrout, P. B. *J. Phys. Chem.* **1995**, *99*, 7819–7828.
(72) Otilia, M.; Manuel, Y.; Jean, Y. S.; Jeanine, T. *Mass Spectrum. Rev.* **2007**, *26*, 474–516.

JP8112045